

Journal Pre-proof

Mixed boundary value problems in power-law functionally graded circular annulus

Dinesh P. Chawde, Tanmay K. Bhandakkar

PII: S0308-0161(21)00098-3
DOI: <https://doi.org/10.1016/j.ijpvp.2021.104402>
Reference: IPVP 104402

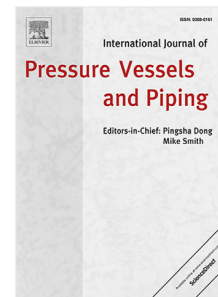
To appear in: *International Journal of Pressure Vessels and Piping*

Received date: 25 January 2021
Revised date: 19 March 2021
Accepted date: 30 March 2021

Please cite this article as: D.P. Chawde and T.K. Bhandakkar, Mixed boundary value problems in power-law functionally graded circular annulus, *International Journal of Pressure Vessels and Piping* (2021), doi: <https://doi.org/10.1016/j.ijpvp.2021.104402>.

This is a PDF file of an article that has undergone enhancements after acceptance, such as the addition of a cover page and metadata, and formatting for readability, but it is not yet the definitive version of record. This version will undergo additional copyediting, typesetting and review before it is published in its final form, but we are providing this version to give early visibility of the article. Please note that, during the production process, errors may be discovered which could affect the content, and all legal disclaimers that apply to the journal pertain.

© 2021 Published by Elsevier Ltd.



Mixed boundary value problems in power-law functionally graded circular annulus

Dinesh P. Chawde

*Research scholar at Indian Institute of Technology Bombay,
Assistant Professor in the Department of Mechanical Engineering,
K J Somaiya College of Engineering
Vidyavihar, Mumbai 400077
Email: dineshc@somaiya.edu*

Tanmay K. Bhandakkar

*Associate Professor
Department of Mechanical Engineering
Indian Institute of Technology Bombay
Powai, Mumbai 400076
Email: tbhanda2@iitb.ac.in*

Abstract

The present work proposes a semi-analytical technique for solution of mixed boundary value problem in functionally graded circular annulus wherein shear modulus varies radially in power-law form while Poisson's ratio is constant. The technique relies on two main steps. In the first step, corresponding to terms in periodic Fourier series applied individually as traction along the annulus surface, stress and displacement field in the annulus is computed harnessing Airy stress functions approach. In the second step, leveraging the strain-displacement relations in polar co-ordinates, mixed boundary conditions are rendered in terms of displacement all along the annulus surface. Assuming the unknown traction along the annulus surface in terms of periodic Fourier series with finite terms, the modified displacement boundary condition, family of solution from the first step and orthogonality of sine and cosine functions is used to generate a system of simultaneous linear equations for the series coefficients. Knowing the coefficients of periodic Fourier series, stress and displacement field can be computed everywhere in the annulus. The first step is digitized in terms of MAPLE functions, exhaustively validated through traction distribution comprising of normal, shear traction

Preprint submitted to International Journal of Pressure Vessel and Piping March 19, 2021

on part of the boundary and pair of equal and diametrically opposite point load along the boundary. The second step is corroborated through a problem where the inner surface is subjected to a specified traction distribution and mixed boundary conditions exist along the outer surface in the form of complete constraint along a part and traction-free condition elsewhere.

Key words: Elasticity; Analytical modelling; Functionally graded circular annulus

1. Introduction

Functionally graded (FG) materials belong to the class of inhomogeneous material wherein the material properties vary smoothly with spatial co-ordinates in a prescribed manner [1, 2]. Many of the naturally occurring materials like nacre, shells are FG and in fact owe their superior mechanical response to the underlying inhomogeneity [3]. Taking a clue from nature and simultaneously aided with advancement in manufacturing technology has led to development of man-made FG materials with applications in the area of rocket engine components [4], protective coatings on turbine blades [5], replacement of damaged bones and teeth in human beings [6–8], bullet-proof vests [9]. Apart from FG materials, layered media [10], composites [11] constitute examples of popular inhomogeneous material systems known to be extremely proficient in serving specific functional requirement. In these systems, the material properties vary discretely which is reflected through the variation in stress and strain field. On the contrary, the continuous variation of material properties in FG materials lead to smooth distribution of stress and strain field. Therefore FG materials have been advocated to serve the dual goal of serving a specific functional requirement and at the same time regulating the stress-levels [1, 12, 13]. The latter in turn reduces the stress-concentration and the concomitant defect nucleation and evolution. Impact of functional grading on contact and fracture response, two of the most important problems in solid mechanics are the subject of many of the recent investigation [14–17].

Noting the influence of functional grading on stress concentration, researchers have tried to design FG material system which minimizes stress concentration. In one approach, the objective is to seek a suitable functional grading [18–20] while in the other approach FG material is explored as a bridging layer in the form of strip or annulus joining two materials [13, 21–26]. Many

of these studies [13, 18–26] are semianalytical in nature owing to the choice of separable geometry and traction boundary conditions (BCs). Consistent in the manner of approach, the present study deals with a two-dimensional circular power-law FG annulus but subjected to arbitrary BCs including *mixed boundary conditions* (MBCs) in a semi-analytical framework. Through the ability to handle all kinds of BCs, the present work is a step towards expanding the scope of the works [13, 18–26]. Before moving onto the next section, the following paragraphs summarize the important work dealing with FG circular annulus to bring forth the absence of similar work in literature.

The mathematical form of the grading assumed for FG circular annulus from literature are linear [27, 57], power-law [28–32], exponential [33, 53–58]. One of the earliest elasticity solutions involving FG annulus dealt with solution to Lamé's problem in an annulus with power-law variation in Young's modulus [31]. Pan and Roy [32] through assumption of separation of variables based solution to displacement-strain-stress field and periodic Fourier series expansion as the functional form in θ direction presented solution to homogeneous and/or FG with power-law grading in elastic modulus multilayered annulus subjected to displacement and/or traction BCs. Jabbari and co-workers [29, 30, 34] provided the thermoelasticity solution in a FG circular annulus with power-law grading while being subjected to thermal and mechanical loads. Li and Peng [28] gave an integral equation based solution for axisymmetric deformation in FG circular annulus with any arbitrary radial variation in elastic properties. In contrast to works discussed till now, focussing on axisymmetric deformation in a FG circular annulus, Batra and co-workers [18–20] dealt with the inverse problem wherein the nature of functional grading was pursued while ensuring either minimization of stress or maximization of stiffness. Adopting approach similar as [32], Nie and Batra [18] assumed the Airy stress function as separable function of radial r and tangential θ co-ordinate with the latter represented through periodic Fourier series terms, and gave a semi-analytical solution for stress and displacement in a FG circular annulus with power-law functional form for elastic modulus and Poisson's ratio and subjected to traction and/or displacement boundary conditions. Li and Liu [27] treated FG circular annulus as equivalent to a number of homogeneous circular annuli perfectly bonded to each other and applied the complex variable approach to latter and gave elasticity solution for traction boundary conditions. The study by Mohammadi et al. [35] on FG cylindrical coatings undergoing axisymmetric deformation concluded that spatial variation of Poisson's ratio can significantly influence the results

for thick cylinders. The idea of having a layer of FG material as a stress controlling measure in circular annulus geometry explored primarily through axisymmetric deformation in [21–26] was extended by Li et al. through generalized bi-axial loading [13] and their study revealed that stress concentration can be reduced substantially as compared to the homogeneous counterpart through tuning of the functional form of grading.

It is evident from the above literature survey concerning FG circular annulus, that none of the works have focussed on MBCs which as a matter of fact describe most of the actual scenarios. Popular numerical approaches like finite element (FE) [36] and boundary element (BE) [37] methods are not restricted by geometry, boundary conditions or material response but being numerical in nature cannot fully replace an analytical solution. Wang and Hasebe [38] have extended the Complex variable method, an extremely powerful and versatile approach in two-dimensional homogeneous elasticity [39] to FG material having constant Poisson's ratio and elastic modulus slightly perturbed from the homogeneous state. The latter condition is restrictive and importantly fails to address FG material with significant gradient. Additionally, the concept of analytic continuation which allows closed form solution of problems with MBCs via Complex variable method is not workable for annulus geometry [40, 41].

The importance of mixed boundary value problems (MBVPs) cannot be overemphasized and the work presented here is a step to redress the existing gap in literature involving MBVPs in FG circular domain. Power-law variation in radius is assumed for shear modulus while the Poisson's ratio is treated as constant. The procedure to **handle** MBVPs on circular domain is decomposed into two steps. In the first step, in a view to replicate Michell solution [42–44] for power-law FG material, solution for displacement and stress in annulus is developed for all distinct and statically meaningful terms in the periodic Fourier series as applied traction along the annulus surface. All these traction cases collectively will be hereafter referred to as standard loading. Under the presumption that any form of applied traction along the annulus surface can be reasonably represented through periodic fourier series with the coefficients extracted through orthogonality of sine and cosine functions, stress and displacement in the annulus can be obtained through linear superposition of the solution corresponding to the standard loading. In case, displacement BCs are prescribed, periodic fourier series with unknown coefficients is considered as the traction along the annulus surface. Using solution corresponding to standard loading, displacement field is assembled

along the annulus surface in terms of the unknown coefficients. Equating the same to known displacement BC and invoking orthogonality, unknown coefficients can be computed and thereby leading to the complete field solution. The solutions associated with standard loading are specialized to cavity in an infinite plane. Now it is important to mention that the approach concerning solution of problems involving traction and displacement BCs discussed above bears similarity with the past works [32] and [18], especially the latter where in fact Poisson's ratio was also assumed to vary radially in power-law form. So without claiming novelty of the process detailed in the first step, it is worthwhile to mention that the steps are laid down very systematically and applied to test cases not discussed in any of these references. Significantly, the outcome of first step is crucial to the second step, where mixed boundary conditions are tackled. The MBC pose a challenge because of the inability to apply orthogonality due to lack of consistently one type of boundary condition. Following Singh and Bhandakkar [41], the strain-displacement relations in polar co-ordinates is exploited to represent traction along the annulus boundary as a linear combination of displacement and its gradients. As a consequence, MBC can be rewritten in terms of displacement all along the annulus boundary and orthogonality can be applied as discussed above while talking about displacement BC case. Due to the presence of unknowns on either side of the modified BC, the unknown coefficients of the periodic Fourier series are realized through solution of a system of simultaneous linear equations.

The outline of the remaining paper is as follows. Next section describes the problem followed by section detailing the solution methodology to generate stress and displacement field tied to standard loading. The subsequent section outlines the steps to apply the solutions for standard loading to traction, displacement and mixed BC cases respectively. It is succeeded by Results and Discussion section where the presented work is adequately validated through the test cases encompassing traction and mixed BCs. Lastly the Conclusions section summarizes the present work.

2. Problem formulation and definition

Fig. 3 shows the cross-section of a linear elastic, isotropic, hollow cylinder of inner radius r_1 , outer radius r_2 possessing a radially varying shear modulus $\mu(r)$ and constant Poisson's ratio ν . The radial variation of μ is assumed to

be power-law and given as [28],

$$\mu(r) = M \left(\frac{r}{r_2} \right)^\beta, \quad (1)$$

where M is the shear modulus of cylinder at radius r_2 and exponent β is the inhomogeneity parameter whose deviation from 0 is the measure of inhomogeneity in the material. The two-dimensional elasticity problem dealt here can be either plane stress ($P\sigma$) or plane strain ($P\epsilon$) depending upon the extent of out-of-plane dimension as compared to the in-plane dimensions and loading variation in the out-of-plane direction. Considering the cylindrical geometry and the cross-section, the associated field quantities in Fig. 3 and the governing equations are described using (r, θ) polar co-ordinates. The radial and tangential components of displacement are denoted by u_r and u_θ while the in-plane components of stress (strain) are $\sigma_r, \sigma_\theta, \sigma_{r\theta}$ ($\epsilon_r, \epsilon_\theta, \epsilon_{r\theta}$) respectively. Under quasi-static conditions and in the absence of body force, the planar equilibrium equations are given as [42, 43],

$$\begin{aligned} \frac{\partial \sigma_r}{\partial r} + \frac{1}{r} \frac{\partial \sigma_{r\theta}}{\partial \theta} + \frac{1}{r} (\sigma_r - \sigma_\theta) &= 0, \\ \frac{\partial \sigma_{r\theta}}{\partial r} + \frac{1}{r} \frac{\partial \sigma_\theta}{\partial \theta} + \frac{2}{r} \sigma_{r\theta} &= 0. \end{aligned} \quad (2)$$

The in-plane strain-displacement relations are given as [43],

$$\epsilon_r = \frac{\partial u_r}{\partial r}, \quad \epsilon_\theta = \frac{u_r}{r} + \frac{1}{r} \frac{\partial u_\theta}{\partial \theta}, \quad \epsilon_{r\theta} = \frac{1}{2} \left(\frac{1}{r} \frac{\partial u_r}{\partial \theta} + \frac{\partial u_\theta}{\partial r} - \frac{u_\theta}{r} \right), \quad (3)$$

and lead to the in-plane strain components being constrained through compatibility condition as [44],

$$\frac{\partial^2 \epsilon_{\theta\theta}}{\partial r^2} + \frac{1}{r^2} \frac{\partial^2 \epsilon_{rr}}{\partial \theta^2} + \frac{2}{r} \frac{\partial \epsilon_{\theta\theta}}{\partial r} - \frac{1}{r} \frac{\partial \epsilon_{rr}}{\partial r} = \frac{2}{r} \frac{\partial^2 \epsilon_{r\theta}}{\partial r \partial \theta} + \frac{2}{r^2} \frac{\partial \epsilon_{r\theta}}{\partial \theta}. \quad (4)$$

The planar form of generalized Hooke's law relating stress and strain com-

ponents is given as [42, 43],

$$\varepsilon_r = \frac{1}{8} \frac{\sigma_r (1 + \kappa) - (3 - \kappa) \sigma_\theta}{\mu(r)}, \varepsilon_\theta = \frac{1}{8} \frac{\sigma_\theta (1 + \kappa) - (3 - \kappa) \sigma_r}{\mu(r)}, \varepsilon_{r\theta} = \frac{1}{2} \frac{\sigma_{r\theta}}{\mu(r)}, \quad (5)$$

where κ is the Kolosov constant equal to $(3 - \nu)/(1 + \nu)$ and $(3 - 4\nu)$ for plane stress (P σ) and plane strain (P ε) deformation respectively.

Specification of boundary conditions (BCs) along with equilibrium equations Eq. (2), strain-displacement relations Eq. (3), stress-strain relation Eq. (5) will complete the description of the elasticity problem [43, 44]. Boundary condition can be provision of either displacement or traction or combination of both traction and displacement along the boundary surface [45]. The latter being termed as mixed boundary conditions (MBCs) and concerns the present work. Thus in general, the boundary conditions for annulus can be written as follows [41]; along radius r_1 ,

$$\begin{aligned} \alpha_{11}(\theta) u_r(r_1, \theta) + \beta_{11}(\theta) \sigma_r(r_1, \theta) &= f_{11}(\theta), \\ \alpha_{12}(\theta) u_\theta(r_1, \theta) + \beta_{12}(\theta) \sigma_{r\theta}(r_1, \theta) &= f_{12}(\theta), \end{aligned} \quad (6)$$

while along the outer radius ($r = r_2$),

$$\begin{aligned} \alpha_{21}(\theta) u_r(r_2, \theta) + \beta_{21}(\theta) \sigma_r(r_2, \theta) &= f_{21}(\theta), \\ \alpha_{22}(\theta) u_\theta(r_2, \theta) + \beta_{22}(\theta) \sigma_{r\theta}(r_2, \theta) &= f_{22}(\theta), \end{aligned} \quad (7)$$

where $\alpha_{11}, \beta_{11}, \alpha_{12}, \beta_{12}, \alpha_{21}, \beta_{21}, \alpha_{22}, \beta_{22}, f_{11}, f_{12}, f_{21}, f_{22}$ are known functions of θ . Displacement BCs are recovered when coefficient $\beta_{ij} = 0$, while traction BCs imply $\alpha_{ij} = 0, i, j = 1, 2$ and $0 < \theta < \pi$. If either of the Eq. (6) or (7) cannot represent the boundary condition singlehandedly throughout the annulus surface, then the boundary conditions represent MBCs.

An obvious approach to solve elasticity problem on FG circular annulus would be to seek generalized stress and displacement field analogous to the Michell solution in homogeneous medium [42–44]. The generalized solution forms the basis function for representation of stress-displacement field in annulus under any set of boundary conditions including MBCs. Consequently the next section discusses the solution methodology to construct the generalized solution for FG annulus and is followed by the procedure to apply it to problems with MBC.

3. Generalized stress-displacement field in FG annulus

The generalized solution for stress and displacement in the elastic FGM annulus can be generated by accounting for all possible traction loading on its boundaries. A reasonably smooth radial ($p(\theta)$) and tangential ($q(\theta)$) traction on the boundaries of the annulus can be adequately represented through periodic Fourier series representation as [46],

$$\begin{aligned} p(\theta) &= p_0 + \sum_{\omega=1}^{\infty} p_{\omega}^c \cos(\omega\theta) + \sum_{\omega=1}^{\infty} p_{\omega}^s \sin(\omega\theta), \\ q(\theta) &= q_0 + \sum_{\omega=1}^{\infty} q_{\omega}^c \cos(\omega\theta) + \sum_{\omega=1}^{\infty} q_{\omega}^s \sin(\omega\theta), \end{aligned} \quad (8)$$

where

$$\begin{aligned} p_0 &= \frac{1}{2\pi} \int_0^{2\pi} p(\theta) d\theta, & p_{\omega}^c &= \frac{1}{\pi} \int_0^{2\pi} p(\theta) \cos(\omega\theta) d\theta, & p_{\omega}^s &= \frac{1}{\pi} \int_0^{2\pi} p(\theta) \sin(\omega\theta) d\theta, \\ q_0 &= \frac{1}{2\pi} \int_0^{2\pi} q(\theta) d\theta, & q_{\omega}^c &= \frac{1}{\pi} \int_0^{2\pi} q(\theta) \cos(\omega\theta) d\theta, & q_{\omega}^s &= \frac{1}{\pi} \int_0^{2\pi} q(\theta) \sin(\omega\theta) d\theta, \end{aligned} \quad (9)$$

and ω is a positive integer. Thus the generalized solution for FGM along the lines of Michell solution can be obtained by deriving the elasticity solution corresponding to each term in the series Eq. (8) in isolation as loading applied at inner and outer boundary of the annulus respectively. Note that except for $\cos \theta$ and $\sin \theta$, every other term in the series regarded as either radial and tangential traction acting along the radial boundary, independently satisfies the force and moment balance for annulus [43] and hence qualify as a statically meaningful loading $\cos \theta$ ($\sin \theta$) and $\sin \theta$ ($\cos \theta$) as radial and tangential load respectively along any radial boundary have to be considered simultaneously to ensure force and moment balance [43] and will be dealt separately. The procedure to derive stress and displacement field is common to all the series terms in Eq. (8) and is illustrated with the example of power-law FG hollow cylinder subjected to radial traction $\cos(n\theta)$, $n \geq 2$ along the inner radius $r = r_1$ and traction free outer surface ($r = r_2$). The BCs are

thus given as,

$$\begin{aligned}\sigma_r(r_1, \theta) &= -\cos(n\theta), & \sigma_{r\theta}(r_1, \theta) &= 0, \\ \sigma_r(r_2, \theta) &= 0, & \sigma_{r\theta}(r_2, \theta) &= 0.\end{aligned}\quad (10)$$

Airy stress function ($\phi(r, \theta)$) method is adopted to further proceed with the solution. The in-plane components of stress are expressed in terms of $\phi(r, \theta)$ as [42, 43],

$$\begin{aligned}\sigma_{\theta}(r, \theta) &= \frac{\partial^2 \phi(r, \theta)}{\partial r^2}, & \sigma_r(r, \theta) &= \frac{1}{r} \frac{\partial \phi(r, \theta)}{\partial r} + \frac{1}{r^2} \frac{\partial^2 \phi(r, \theta)}{\partial \theta^2}, \\ \sigma_{r\theta}(r, \theta) &= \frac{1}{r^2} \frac{\partial \phi(r, \theta)}{\partial \theta} - \frac{1}{r} \frac{\partial^2 \phi(r, \theta)}{\partial r \partial \theta},\end{aligned}\quad (11)$$

and ensure the satisfaction of equilibrium equations (Eq. (2)). Combining Eqs.(4), (5), and (11) leads to the following governing equation for $\phi(r, \theta)$,

$$\begin{aligned}& \left[(\kappa - 3)r^3 \frac{\partial \phi(r, \theta)}{\partial r} + (\kappa - 3)r^2 \frac{\partial^2 \phi(r, \theta)}{\partial \theta^2} + (\kappa + 1)r^4 \frac{\partial^2 \phi(r, \theta)}{\partial r^2} \right] \mu(r) \frac{d\mu(r)}{dr} \\ & + \left[(-2\kappa + 6)r^3 \frac{\partial \phi(r, \theta)}{\partial r} + (-2\kappa + 6)r^2 \frac{\partial^2 \phi(r, \theta)}{\partial \theta^2} + (-2\kappa - 2)r^4 \frac{\partial^2 \phi(r, \theta)}{\partial r^2} \right] \\ & \left(\frac{d\mu(r)}{dr} \right)^2 + \left[(2\kappa + 2)r^2 \frac{\partial^3 \phi(r, \theta)}{\partial \theta^2 \partial r} + (2\kappa + 2)r^4 \frac{\partial^3 \phi(r, \theta)}{\partial r^3} - (\kappa + 1)r^2 \frac{\partial \phi(r, \theta)}{\partial r} \right. \\ & - (3\kappa + 3)r \frac{\partial^2 \phi(r, \theta)}{\partial \theta^2} + (3\kappa - 1)r^3 \frac{\partial^2 \phi(r, \theta)}{\partial r^2} \left. \right] \mu(r) \frac{d\mu(r)}{dr} - \left[(2\kappa + 2)r^3 \frac{\partial^3 \phi(r, \theta)}{\partial r^3} \right. \\ & - (2\kappa + 2)r^2 \frac{\partial^4 \phi(r, \theta)}{\partial \theta^2 \partial r^2} + (2\kappa + 2)r \frac{\partial^3 \phi(r, \theta)}{\partial \theta^2 \partial r} - (\kappa + 1) \frac{\partial^4 \phi(r, \theta)}{\partial \theta^4} \\ & - (\kappa + 1)r^4 \frac{\partial^4 \phi(r, \theta)}{\partial r^4} - (\kappa + 1)r \frac{\partial \phi(r, \theta)}{\partial r} + (-4\kappa - 4) \frac{\partial^2 \phi(r, \theta)}{\partial \theta^2} + \\ & \left. (\kappa + 1)r^2 \frac{\partial^2 \phi(r, \theta)}{\partial r^2} \right] (\mu(r))^2 = 0\end{aligned}\quad (12)$$

Note that the substitution of $\beta = 0$ in Eq. (1) reduces Eq. (12) to the well-known biharmonic equation for Airy stress function in homogeneous medium [42–44]. Given a smooth function $f(\theta)$ of periodic variable θ , its

periodic Fourier transform $\bar{f}(\omega)$ is given as [46],

$$\bar{f}(\omega) = \int_0^{2\pi} f(\theta) \exp(-i\omega\theta) d\theta \quad (13)$$

where ω is an integer and $i = \sqrt{-1}$. Note that the fourier transform of a function is denoted by an overhead bar over the function symbol. ω appearing in Eq. (13) has no connection with the one in Eq. (9) except for the fact that both are positive integers. The inverse fourier transform to retrieve back the original function is [46],

$$f(\theta) = \frac{1}{\pi} \int_0^{2\pi} \bar{f}(\omega) d\omega \quad (14)$$

Exploiting the periodic nature of the resulting solution, the partial differential equation (pde) Eq. (12) can be reduced by applying periodic fourier transforms as,

$$\begin{aligned} & - (1 + \kappa)r^4 \frac{d^4 \bar{\phi}(r, \omega)}{dr^4} + 2(1 + \kappa)(\beta - 1)r^3 \frac{d^3 \bar{\phi}(r, \omega)}{dr^3} \\ & + (-\beta^2 \kappa + 2k\omega^2 - \beta^2 + 2\beta\kappa + 2\omega^2 - 2\beta + \kappa + 1)r^2 \frac{d^2 \bar{\phi}(r, \omega)}{dr^2} \\ & + (1 + \beta)(-2\kappa\omega^2 - \beta\kappa - 2\omega^2 + 3\beta - \kappa - 1)r \frac{d\bar{\phi}(r, \omega)}{dr} \\ & + \omega^2(\beta^2 \kappa - \kappa\omega^2 - 3\beta^2 + 4\beta\kappa - \omega^2 + 4\kappa + 4)\bar{\phi}(r, \omega) = 0. \end{aligned} \quad (15)$$

It is noted that the above Eq. (15) is the well-known homogeneous Cauchy-Euler ordinary differential equation (ode) in r with solution of the form r^m [46]. Substituting the proposed power-law solution for $\bar{\phi}(r, \omega)$ in Eq. 15 gives the following quartic equation in the unknown exponent m ,

$$\begin{aligned} & (1 + \kappa)m^4 + (-2\beta\kappa - 2\beta - 4\kappa - 4)m^3 + \\ & (\beta^2 \kappa - 2\kappa\omega^2 + \beta^2 + 4\beta\kappa - 2\omega^2 + 8\beta + 4\kappa + 4)m^2 + \\ & (2\beta\kappa\omega^2 + 2\beta\omega^2 + 4\kappa\omega^2 - 4\beta^2 + 4\omega^2 - 8\beta)m + \\ & (-\beta^2 \kappa\omega^2 + k\omega^4 + 3\beta^2\omega^2 - 4\beta\kappa\omega^2 + \omega^4 - 4\kappa\omega^2 - 4\omega^2) = 0 \end{aligned} \quad (16)$$

with roots $m_i, i = 1, 2, 3, 4$ obtained via symbolic software MAPLE[©],

$$\begin{aligned} m_1 &= P(\omega) + Q(\omega), & m_2 &= P(\omega) - Q(\omega), \\ m_3 &= P(\omega) + R(\omega), & m_4 &= P(\omega) - R(\omega), \end{aligned} \quad (17)$$

where $P(\omega), Q(\omega), R(\omega)$ are given as,

$$\begin{aligned} P(\omega) &= \frac{\beta}{2} + 1, \quad Q(\omega) = \frac{Q_1(\omega)}{2(1 + \kappa)}, \quad Q_1(\omega) = \sqrt{(\kappa + 1)(T_1 + T_2)}, \\ T_1 &= 4[(\beta + 2)^2(\omega\kappa)^2 - 2(\beta^2 - 4)\omega^2\kappa + (\beta + 2)(2 - 3\beta)\omega^2 + 4\beta^2]^{1/2}, \\ T_2 &= (\kappa + 1)[\beta^2 + 4\omega^2 + 4] - 4(\kappa - 1)\beta, \end{aligned}$$

$$\begin{aligned} R(\omega) &= \frac{1}{2} \sqrt{\frac{(R_1 + R_2)}{(\kappa + 1)}}, \\ R_1 &= -4 \sqrt{((\kappa - 3)\beta + 2\kappa + 2)(\beta + 2)(\kappa + 1)\omega^2 + 4\beta^2}, \\ R_2 &= (\beta^2 + 4\omega^2 + 4\beta + 4)\kappa + \beta^2 + 4\omega^2 - 4\beta + 4. \end{aligned}$$

Thus the solution of Eq. (15) in fourier domain is,

$$\bar{\phi}(r, \omega) = C_1(\omega)r^{m_1} + C_2(\omega)r^{m_2} + C_3(\omega)r^{m_3} + C_4(\omega)r^{m_4} \quad (18)$$

where $C_1(\omega), C_2(\omega), C_3(\omega), C_4(\omega)$ are constants to be determined based on the boundary conditions at the inner ($r = r_1$) and outer ($r = r_2$) boundary respectively. Applying periodic Fourier transform to the boundary conditions Eq. (10) of the illustrative problem,

$$\begin{aligned} \bar{\sigma}_r(r_1, \omega) &= \pi[\delta(n + \omega) + \delta(n - \omega)], \quad \bar{\sigma}_{r\theta}(r_1, \omega) = 0, \\ \bar{\sigma}_r(r_2, \omega) &= 0, \quad \bar{\sigma}_{r\theta}(r_2, \omega) = 0, \end{aligned} \quad (19)$$

where $\delta()$ is the Dirac Delta function [45]. Combining Eqs.(13) and (15), the relationship between Airy stress function ϕ and stress-components in Fourier

domain is,

$$\begin{aligned}\bar{\sigma}_\theta(r, \omega) &= \frac{d^2 \bar{\phi}(r, \omega)}{dr^2}, & \bar{\sigma}_r(r, \omega) &= \frac{1}{r} \frac{d \bar{\phi}(r, \omega)}{dr} - \frac{\omega^2}{r^2} \bar{\phi}(r, \omega), \\ \bar{\sigma}_{r\theta}(r, \omega) &= \frac{1}{r^2} \frac{d \bar{\phi}(r, \omega)}{dr} - \frac{i\omega}{r} \frac{d \bar{\phi}(r, \omega)}{dr}.\end{aligned}\quad (20)$$

Substituting BCs from Eq. (19) in Eq. (20) and using the solution for $\bar{\phi}$ given in Eq. (18) leads to a system of four simultaneous linear equations in $C_1(\omega), C_2(\omega), C_3(\omega), C_4(\omega)$ which were solved symbolically in MAPLE[©] to reveal the closed form solution of the integration constants $C_1(\omega), C_2(\omega), C_3(\omega), C_4(\omega)$.

Knowing $C_1(\omega), C_2(\omega), C_3(\omega), C_4(\omega)$, Eqs. (18) and (20) can be used to deduce the in-plane stress components in Fourier domain. The components in physical domain can be computed by applying inverse Fourier transform Eq. (14) and utilizing the "Sifting" property of Dirac delta function [46],

$$\int_0^{2\pi} \bar{f}(\omega) \delta(n \pm \omega) d\omega = \bar{f}(\mp n). \quad (21)$$

Knowing the stresses, strains can be computed based on Eq. (5) and followed by integration of strain-displacement relationship Eq. (3) to yield displacement sans rigid body motion terms [43]. The expressions being lengthy are provided in Supplementary file. The combination of cosine or sine function ($n \geq 2$) as normal or shear traction applied along inner or outer radius leads to eight possibilities. The procedure illustrated above is applied to these eight combinations and the result is compiled as a set of eight independent MAPLE[©] software based functions which outputs in-plane stress and displacement components in polar co-ordinates for a given n . The steps and its sequence is graphically spelled out in the form of flowchart given in Fig. 1. The case of $p(\theta) = p_0$ corresponds to the well-known Lamé's problem and leads to θ independent axisymmetric deformation. The closed form solution to Lames's problem for power-law graded annulus is available in the literature having derived using Fredholm integral equation [28], Airy stress function [19] and is summarized below for completeness. Owing to θ independence, the

governing equation Eq. (12) reduces to,

$$\begin{aligned}
 & -(\kappa + 1)r^4 \frac{d^4\phi(r)}{dr^4} + (2\beta\kappa + 2\beta - 2\kappa - 2)r^3 \frac{d^3\phi(r)}{dr^3} \\
 & + (-\beta^2\kappa - \beta^2 + 2\beta\kappa - 2\beta + \kappa + 1)r^2 \frac{d^2\phi(r)}{dr^2} \\
 & + (-\beta^2\kappa + 3\beta^2 - 2\beta\kappa + 2\beta - \kappa - 1)r \frac{d\phi(r)}{dr} = 0 \quad (22)
 \end{aligned}$$

which is also a Cauchy-Euler ODE with $1, r^{\beta+2}, r^\alpha, r^{\beta+2-\alpha}$ as the fundamental solutions (MAPLE 18), where α is given as,

$$\alpha = 1 + \frac{\beta}{2} + \frac{[(\kappa + 1)(\beta + 2)^2 - 16\beta]^{1/2}}{2\sqrt{\kappa + 1}} \quad (23)$$

The first two solutions are discarded as they violate the requirement of zero tangential displacement u_θ in an axisymmetric deformation. Thus the feasible solution of Airy stress function for the case of constant normal pressure along inner and outer boundaries is,

$$\phi(r) = C_3 r^\alpha + C_4 r^{\beta+2-\alpha}, \quad (24)$$

where C_3, C_4 are arbitrary constants to be determined based on the applied pressure along the boundary. Applying Eq. (11) in combination with Eq. (24), the non-zero in-plane stresses are,

$$\begin{aligned}
 \sigma_r &= C_3 \alpha r^{\alpha-2} + (\beta - \alpha + 2)C_4 r^{\beta-\alpha}, \\
 \sigma_\theta &= C_3 \alpha(\alpha - 1)r^{\alpha-2} + (\beta - \alpha + 2)(\beta - \alpha + 1)C_4 r^{\beta-\alpha}. \quad (25)
 \end{aligned}$$

Consideration of first term in the R.H.S of Eq. (8) as loading amounts to,

$$\sigma_r(r_1) = -p_1, \quad \sigma_r(r_2) = -p_2, \quad (26)$$

as boundary conditions. Eqs. (25) and (26) can be solved together to yield the values of the unknown constants C_3 and C_4 . Knowing the stresses, strain (Eq. (5)) and subsequently displacements (Eq. (3)) can be computed. The expressions being lengthy are not provided here but it was ensured that they confirm with the available solution for the Lames problem in literature

[18, 28, 58], as well as the homogeneous solution ($\beta = 0$) [43, 44]. These solutions are converted into two MAPLE[©] software functions which yield the in-plane stresses and displacement in the circular annulus while being subjected to internal and external pressure respectively.

In contrast with the constant pressure case, the case of constant shear traction q_0 along a radial surface cannot exist on its own and hence is not a valid loading for solid disc ($r_1 = 0$). In the case of annulus, a constant shear traction of q_1 along the inner radius $r = r_1$ demands a constant shear traction of $-(r_1/r_2)^2 q_1$ to be applied along the outer radius to ensure moment balance [43]. Through invocation of moment balance on an annulus of inner radius r_1 and outer radius $r < r_2$ and equilibrium equations (Eq. (2)), it can be concluded that the stress field for constant shear traction along annulus is,

$$\sigma_r = 0, \quad \sigma_{r\theta}(r, \theta) = q_1 \left(\frac{r_1}{r} \right)^2, \quad \sigma_\theta = 0. \quad (27)$$

Note that the above solution is independent of β and in fact upholds for any material response of annulus. Combination of Eqs. (27), (5) and (3) followed by integration leads to the displacement field as,

$$u_r(r, \theta) = 0, \quad u_\theta(r, \theta) = \frac{q_1}{M} \frac{r_1^2 r_2^\beta}{r^{\beta+1}}. \quad (28)$$

For $\beta = 0$, the displacement field in Eq. (28) confirms with the solution for homogeneous material [43]. Eqs. (27) and (28) are also converted into a MAPLE[©] function for constant shear traction along the annulus surface.

As discussed earlier, $\cos \theta$ or $\sin \theta$ cannot be the standalone normal or tangential traction acting along the annulus surface. Rather a combination of $\cos \theta$ ($\sin \theta$) and $\sin \theta$ ($\cos \theta$) as normal and tangential traction respectively along a radial surface is necessary to ensure force and moment balance [43]. Accounting for inner and outer surfaces and combination of cosine and sine functions, a total of four loading scenarios ensue and were solved repeating the procedure demonstrated via the solution of the example with BCs given by Eq. (10). The four cases are also coded as MAPLE[©] functions to complete all the loading possibilities for an annulus as dictated by Eq. (8). A compilation of all the MAPLE[©] functions constitutes the generalized Michell function for power-law FG linear elastic circular annulus and signifies the first major contribution of the present work.

3.1. Infinite plane with circular cavity

The geometry of an infinite plane with circular cavity can be recovered from the annulus in the limit of outer radius $r_2 \rightarrow \infty$. Procedure wise, there is no change owing to the domain modification but the requirement of bounded stress and displacement field at infinity necessitates the exponent in the power-law solution to be non-positive. So amongst the four possibilities for exponent expressed in Eq. (17), two of the values have to be discarded on account of their non-negativity. Since the sign of roots depend on β and n in the applied loading, to identify the roots to be disposed of, following strategy was utilized. It was graphically checked that for feasible values of β and any n , amongst the four roots given in Eq. (17), $m_1 > 0, m_2 < 0$ regardless of the sign of β , while the roots $m_3 > 0, m_4 < 0$ for $\beta > 0$ and viceversa. Thus depending upon whether β is positive or negative, $\{m_2, m_4\}$ or $\{m_2, m_3\}$ respectively are the relevant roots for the infinite domain with circular cavity. For the case of traction specified along the cavity surface, using the two appropriate roots, the Airy stress function in Eq. (18) can be proceeded along the same lines as finite annulus for calculation of stresses and displacement in the infinite plane with cavity. If the loading on the cavity is axisymmetric, only one root out of $\{m_1, m_2, m_3, m_4\}$ is relevant. Graphical check for feasible values of β led to m_3 in Eq. (17) as the sole root for finite stresses and displacement.

4. Solution strategy for BVP in power-law FG annulus

The present section describes the steps to be undertaken to calculate stress and displacement in the power-law FG annulus corresponding to traction, displacement and mixed BCs on the annulus surface.

4.1. Traction BVP

In case, the traction distribution on the inner and/or outer surface of annulus i.e. $\alpha_{ij} = 0$ in Eqs. (6, 7) is prescribed, the steps to compute stresses and displacement in the annulus is as follows:

- a) The given traction is resolved in the radial ($p(\theta)$) and tangential ($q(\theta)$) direction respectively.
- b) Following Eqs. (8 - 9), the loading at inner and/or outer surface is represented in terms of its periodic Fourier representation. Depending upon the applied loading, the upper range in the summation sign is terminated at a finite number N to ensure convergence of the ensuing series for displacement

and stress components.

c) The Maple[©] functions for stress and displacement field in the annulus corresponding to the periodic Fourier function as radial and/or tangential loading at the inner and/or outer surface dealt in previous section are invoked.

d) Applying the principle of superposition [42, 43], the stress and displacement components corresponding to each Maple[©] function are amplified with the respective Fourier series coefficient and added to yield the requisite solution.

A series of loading scenarios are dealt in the Results and Discussion section to validate the above procedure and the MAPLE[©] functions via comparison with an independent finite element (FE) simulation in ABAQUS [47].

4.2. Displacement BVP

In case the boundary conditions along the annulus surface is in terms of displacement i.e. $\beta_{ij} = 0$, then the Mitchell solution derived for power-law FGM can be applied as follows:

(a) Expression described by the periodic Fourier series in the right hand side of Eqs.(8-9) is assumed as the radial and tangential loading on the annulus surface with the infinite sum truncated at a reasonable N value. Thus barring the case of constant shear traction, for a given N , the total number of coefficients and functions to be handled are $2(N - 1) + 1 + 2(N - 1) + 2 = 4N - 1$.

(b) Using the Maple[©] function corresponding to each functional term in the expression of Eqs. (8-9) at the appropriate (inner or outer) surface, the displacement field is expressed in terms of the unknown coefficients.

(c) The displacement field along the (inner/outer) surface is equated to the given boundary condition and summoning the orthogonality property of sine and cosine functions, the coefficients can be extracted.

(d) The value of N in step (a) is decided to ensure convergence of series in the solution of stress and displacement field.

(e) The contribution to displacement field from the loading at the boundary other than the one where displacement BC is applied should also be accounted.

4.3. Mixed BVP

The method of expressing traction along boundary surface in terms of periodic Fourier series and then proceeding with Maple[©] based Mitchell

functions cannot be implemented for MBCs as the form of BC is not consistent throughout $[0, 2\pi]$. The issue can be resolved by reexpressing the BCs consistently in terms of displacements [41] through combined application of stress-strain and strain-displacement relationship. For instance, Eqs.(3, 5) allows the boundary condition Eq. (6) at inner radius r_1 to be written as follows [41],

$$u_r(r_1, \theta) = \frac{r_1 \left((\kappa - 1)f_{11} - \beta_{11} \left[\mu(r)(\kappa + 1) \frac{\partial u_r}{\partial r} + \frac{1}{r_1} \frac{\partial u_\theta}{\partial \theta} \right]_{r=r_1} \right)}{r_1 \alpha_{11} (\kappa - 1) + \mu(r)(3 - \kappa)},$$

$$u_\theta(r_1, \theta) = \frac{r_1 \left(f_{12} - \beta_{12} \mu(r) \left[\frac{1}{r_1} \frac{\partial u_r}{\partial \theta} + \frac{\partial u_\theta}{\partial r} \right]_{r=r_1} \right)}{r_1 \alpha_{12} - \mu(r) \beta_{12}}, \quad (29)$$

along the outer radius r_2 as,

$$u_r(r_2, \theta) = \frac{r_2 \left((\kappa - 1)f_{21} - \beta_{21} \left[\mu(r)(\kappa + 1) \frac{\partial u_r}{\partial r} + \frac{1}{r_2} \frac{\partial u_\theta}{\partial \theta} \right]_{r=r_2} \right)}{r_2 \alpha_{21} (\kappa - 1) + \mu(r)(3 - \kappa)},$$

$$u_\theta(r_2, \theta) = \frac{r_2 \left(f_{22} - \beta_{22} \mu(r) \left[\frac{1}{r_2} \frac{\partial u_r}{\partial \theta} + \frac{\partial u_\theta}{\partial r} \right]_{r=r_2} \right)}{r_2 \alpha_{22} - \mu(r) \beta_{22}}, \quad (30)$$

Similar reexpressions for BCs in terms of displacement can be achieved for Eqs. (7). Once the BC is expressed in terms of displacement as in Eq. (29, 30) the method to solve MBV on a given surface is as follows:

(a) Analogous to the case of displacement BC in previous section, expression in Eqs. (8, 9) is assumed as the traction distribution with a suitable choice of N for the upper limit in the infinite sum, leading to the total number of unknown coefficients equal to $4N - 1$. The BC at the other radius of the annulus will ascertain whether the constant shear traction term has to be considered or not.

(b) Corresponding to the functional terms in Eqs. (8-9) as radial or tangential traction at the desired (inner/outer) surface, the relevant Maple[®] based Mitchell functions are called and the displacement field is assembled in terms of the unknown coefficients in Eqs. (8-9). The displacement field u_r and u_θ

is further appended with $(A \cos \theta + B \sin \theta)$ and $(-A \sin \theta + B \cos \theta + Cr)$ respectively to acknowledge rigid body translation A, B along the cartesian co-ordinates and small anticlockwise rotation C about the origin.

(c) The expression for displacement field at the MBC surface is evaluated and substituted in the reformulated BC (e.g. in Eq. (29)). Due to the presence of displacement and/or its gradient on either side, unknown coefficients appear on both sides of the reformulated equation. A system of $2(1 + 2N) = 4N + 2$ simultaneous linear equations is generated by appealing to orthogonality property of sine and cosine functions. The difference of 3 between the number of equations and unknown coefficients is accounted by the rigid motion terms A, B, C mentioned in item (b).

(d) The linear equations are assembled and solved to reveal the coefficients.

(e) Note that the contribution to displacement from the surface other than the one where MBC is applied should also be accounted while carrying out step (c).

It was found that the process of assembling the complete displacement field followed by orthogonality to form the system of equations was very time consuming and became unmanageable if N was chosen greater than 30. Instead, a parallelization approach was adopted, wherein each loading was considered separately and the sequence of operation was reversed i.e. orthogonality was followed by assembly. The displacement field for a given standard loading in Eqs. (8-9) was substituted in reformulated BC (e.g. Eq. (29)) and orthogonality w.r.t. $1, \cos(\omega\theta), \sin(\omega\theta), \omega = \{1, 2, \dots, N\}$ was applied on it and the result was stored in a matrix at a designated place. The same process was repeated for all the standard loading in Eqs. (8-9) taking care of appending the result for each step at the appropriate place in the matrix. The matrix was inputted to the linear solver in Maple[©] to get the unknown coefficients corresponding to the standard loading in Eqs. (8-9). Once the coefficients are known, displacement and stress field anywhere in the annulus can be calculated. The steps are also elucidated through the flowchart in Fig. 2. The validity of the above process will be demonstrated through a MBV problem on annulus in next section.

5. Results and Discussion

5.1. Traction BVP

The correctness of Maple[©] functions for the standard loading and the approach enlisted in the previous section will be firstly demonstrated through

the following traction BVPs discussed below.

i) *Uniform pressure p applied along two symmetric arcs of the inner radius r_1 of an annulus as shown in Fig. 3a:*

The BCs along the inner r_1 is,

$$\begin{aligned} \sigma_r(r_1, \theta) &= \begin{cases} -p, & 0 \leq \theta \leq \alpha, \quad \pi - \alpha \leq \theta \leq \pi + \alpha, \quad 2\pi - \alpha \leq \theta \leq 2\pi, \\ 0, & \alpha < \theta < \pi - \alpha, \quad \pi + \alpha < \theta < 2\pi - \alpha, \end{cases} \\ \sigma_{r\theta}(r_1, \theta) &= 0, \quad 0 \leq \theta \leq 2\pi, \end{aligned} \quad (31)$$

and along outer radius $r = r_2$ is,

$$\sigma_r(r_2, \theta) = 0, \sigma_{r\theta}(r_2, \theta) = 0, \quad 0 \leq \theta \leq 2\pi. \quad (32)$$

Following the procedure listed in sub-section 4.1, the radial traction at the inner surface (Eq. (31a)) is expressed as a periodic Fourier series and coupled with the Maple[©] functions for the standard radial loading at the inner annulus surface, the stress and displacement field in the annulus is generated. Solution is explicitly calculated for $p = 1, \alpha = \pi/4, M = 0.385, r_1 = 0.5, r_2 = 1, \nu = 0.3, \beta = 2, N = 100$ assuming plane stress deformation. Owing to the discontinuous nature of loading, the periodic Fourier series and subsequently the series solution to stress and displacement exhibits oscillations near the discontinuity, an undesirable feature well known as Gibb's phenomenon [48]. In fact the frequency and amplitude of oscillations grows with the number of terms N in the series. However the oscillations can be eliminated by the application of filtering and in this work, Lanczos filtering scheme is adopted [41, 48, 49]. Accordingly the coefficient of constant, *sine* and *cosine* function in $p(\theta)$ and $q(\theta)$ of Eqs.(8) are post multiplied with the factor $\sin(\omega\pi/N)/(\omega\pi/N)$ known as sigma factor [48] and the modified factors are used for calculation of stresses and displacement anywhere in the annulus. Hereafter it will be explicitly mentioned if filtering is used to compute and display result in this work.

The result based on the current work are compared against the finite element (FE) simulation carried out in ABAQUS ver. 6.11 [47]. Symmetry of the problem (Fig 3a) about x and y axes is exploited and ergo quarter model is implemented in ABAQUS. Temperature dependence of elastic properties is a well-known method to simulate FGM response within FE software [50]

and the same has been borrowed here. The details are briefly described in Appendix A. FE mesh comprising of 23600, 4 noded Continuum Plane stress element (CPS4) [47] is used to ensure converged result. The meshing was done uniformly using the "Structured Form" feature in ABAQUS [47] such that the smallest element size is 0.005 along the radial direction. Fig. 4 show an excellent match for the in-plane stress and displacement components along a representative path viz. radial line inclined at an angle of 21.36° with respect to the x -axis acquired from the present work (solid line) and FE solution (circular markers). Note that σ_r and $\sigma_{r\theta}$ do satisfy the BCs given in Eq. (31).

ii) *Inner surface r_1 of the annulus subjected to equal and opposite point load F at the diameter ends as shown in Figure 3b:*

The problem of concentrated point load along the annulus can be solved as a special case of the previous problem. The net resultant of uniform pressure $p = F/(2r_1 \sin \alpha)$ in Fig. 3a is horizontal force F acting along the x -axis in the direction of $+x$ ($-x$) axis for the loaded arc region to the right (left) of the y -axis. Thus the solution corresponding to Fig. 3b can be recovered by replacing p with $F/(2r_1 \sin \alpha)$ in the solution to the previous problem (Fig. 3a) followed by applying limit $\alpha \rightarrow 0$ [44]. The calculation is worked out for $r_1 = 1, r_2 = 2, F = 1, M = 0.385, \nu = 0.3, \beta = -2, N = 400$ assuming plane stress deformation. With regards to FE solution, symmetry allows a quarter model subjected to point load $F/2$ sufficient for analysis. "Free Form" feature based mesh comprising of 8737 CPS4 elements were used with very fine mesh near the point load with smallest element size 0.16 to guarantee mesh convergence. Figs. 5 and 6 show comparison of the tangential stress σ_θ and displacement component along the radial path overlapping with x -axis ($\theta = 0$) and along the inner radius $r = r_1$ respectively based on the current approach (solid line) and FE simulation (circular marks). Owing to the symmetry, tangential component of displacement u_θ is identically zero along the x -axis and hence not shown in Fig. 5. Similarly appealing to angular symmetry, results are displayed for $\theta = [0, \pi/2]$ in Fig. 6. The classical $1/r$ singularity in the stress-field due to application of point load [42–44] is signalled from the sudden rise in the magnitude of σ_θ as $r \rightarrow r_1$ and $\theta \rightarrow 0$. But being a series solution, the functional form of the singularity can't be deciphered independently no matter what value of N is used [41].

iii) *Uniform tangential traction q_1 acting along two equal and opposite arcs of the inner radius r_1 with subtended angle 2α countered by traction $q_2 = q_1(r_1/r_2)^2$ in the opposite sense along concentric arcs with same subtended*

angle 2α on the outer radius r_2 as shown in Fig. 3c:

Based on Fig. 3c, the boundary conditions along inner radius $r = r_1$ are,

$$\sigma_r(r_1, \theta) = 0, \quad (33)$$

$$\sigma_{r\theta}(r_1, \theta) = \begin{cases} q_1, & -\alpha < \theta < \alpha, \\ 0, & \alpha < \theta < 2\pi - \alpha, \end{cases} \quad (34)$$

and along outer radius $r = r_2$ are,

$$\sigma_r(r_2, \theta) = 0, \quad (35)$$

$$\sigma_{r\theta}(r_2, \theta) = \begin{cases} q_1(r_1/r_2)^2, & -\alpha < \theta < \alpha, \\ 0, & \alpha < \theta < 2\pi - \alpha. \end{cases} \quad (36)$$

Recapping the procedure listed in sub-section 4.1, the coefficients of the periodic Fourier series for the non-zero tangential traction are computed and aided with Maple[®] function for the standard tangential loading along the inner and outer surfaces, the stress and displacement field in the annulus for Fig. 3c is developed. In particular, the results are computed for $\alpha = \pi/6, r_1 = 2, r_2 = 4, \beta = 1.5, M = 0.385, \nu = 0.3, N = 100$ assuming plane stress deformation. Symmetry consideration allows half model for FE calculations. The mesh comprises of 21105 CPS4R elements with a fine mesh (element with size ~ 0.03) in the region around the point of discontinuity in tangential traction. Fig. 7 demonstrates excellent comparison between the prediction based on the present approach (solid line) and FE solution (circular markers) for the in-plane shear stress $\sigma_{r\theta}$ along the horizontal radial line overlapping with the $+x$ -axis.

Having demonstrated the capability of the current work in solving a variety of traction BVP, the next sub-section will consider a MBVP.

5.2. Mixed BVP

Fig. 3d shows a hollow linear elastic cylinder made of power-law FGM (1) whose inner surface ($r = r_1$) is subjected to a prescribed radial traction $p_1(\theta) = \sin(3\theta) + \cos(2\theta)$ and tangential traction $q_1(\theta) = \cos(3\theta) + \sin(2\theta)$ while the outer surface ($r = r_2$) is subjected to mixed bc i.e. a portion of surface ($\alpha < \theta < 2\pi - \alpha$) is traction-free while the remaining portion ($0 < \theta < \alpha; 2\pi - \alpha < \theta < 2\pi$) is constrained.

The BCs for the Fig. 3d are given as:

$$\begin{aligned} \sigma_r(r_1, \theta) &= -p_1(\theta), & \sigma_{r\theta}(r_1, \theta) &= -q_1(\theta), & 0 < \theta < 2\pi, \\ \sigma_r(r_2, \theta) &= 0, & \sigma_{r\theta}(r_2, \theta) &= 0, & \alpha < \theta < 2\pi - \alpha, \\ u_r(r_2, \theta) &= 0, & u_\theta(r_2, \theta) &= 0, & -\alpha < \theta < \alpha. \end{aligned} \quad (37)$$

It should be noted that the same problem was dealt in a homogeneous medium (i.e. $\beta = 0$) by [41] and their results are used for validation of the present work and at the same time used as a base-line to contrast result of the same problem with $\beta \neq 0$ to bring forth the effect of functional grading on stress and displacement field. The stress-field is known to exhibit square-root singularity with oscillating multipliers as the location along the surface where BC switches from traction to displacement type is approached [41, 51]. In Fig. 3d, at locations $\theta = \alpha$ and $2\pi - \alpha$ along $r = r_2$, the change in the type of BC occurs and hence here after these two locations are referred to as singular points.

As described in sub-section 4.3, the MBCs in Eq. 37, are rewritten in terms of displacement u_r, u_θ . Comparing Eq. 37 with Eq. 7, $\alpha_{21} = \alpha_{22} = 1$ for $-\alpha < \theta < \alpha$ and 0 for $\alpha < \theta < 2\pi - \alpha$, $\beta_{21} = \beta_{22} = 0$ for $-\alpha < \theta < \alpha$ and 1 for $\alpha < \theta < 2\pi - \alpha$, $f_{21} = f_{22} = 0$ for $0 < \theta < 2\pi$. Hence employing Eq. 30, the modified form of MBCs for Fig. 3d are,

$$\begin{aligned} u_r(r_2, \theta) &= \begin{cases} 0, & -\alpha < \theta < \alpha, \\ -\frac{r_2}{\nu} \frac{\partial u_r}{\partial r} \Big|_{r=r_2} - \frac{\partial u_\theta}{\partial \theta} \Big|_{r=r_2}, & \alpha < \theta < 2\pi - \alpha, \end{cases} \\ u_\theta(r_2, \theta) &= \begin{cases} 0, & -\alpha < \theta < \alpha, \\ \frac{\partial u_r}{\partial \theta} \Big|_{r=r_2} + r_2 \frac{\partial u_\theta}{\partial r} \Big|_{r=r_2}, & \alpha < \theta < 2\pi - \alpha. \end{cases} \end{aligned} \quad (38)$$

In-line with the procedure described in sub-section 4.1, firstly the inner surface $r = r_1$ is considered. The given traction is expressed as Fourier periodic series (Eqs. (6-7)), to find out the respective Fourier series coefficients. The MAPLE[©] functions corresponding to the non-zero coefficients are called, amplified with the coefficient value, summed to form contribution to the stress and displacement field due to loading at the inner surface $r = r_1$. The outer surface $r = r_2$ is subjected to MBCs and the procedure reported in sub-section 4.3 is adopted. Traction along radial and tangential direction at $r = r_2$ is assumed as a periodic Fourier series with a reasonable high N value. Note that to start with the coefficients $\{p_0, p_1^c, p_1^s, p_\omega^c, p_\omega^s, q_\omega^c, q_\omega^s\}$,

$\omega = 2, 3, \dots, N$ are unknown. q_0 is non-zero and predecided based on the presence and value of constant part in the given tangential traction at the inner surface $r = r_1$. As described earlier, $p_1^c = q_1^s$ and $p_1^s = q_1^c$ for ensuring force and moment balance of annulus. The MAPLE[©] functions related to the unknown coefficients are called, augmented with the unknown coefficients to express contribution to stress and displacement field due to the outer surface. The total displacement at $r = r_2$ stems from the result of known inner surface contribution, outer surface contribution expressed in terms of the unknown coefficients and the 3 rigid body terms A, B, C . This displacement and its gradient with respect to r and θ evaluated at $r = r_2$ is substituted in Eq. (30) and then subjected to orthogonality to generate $4N + 2$ equations for $4N + 2$ unknowns. As detailed earlier, owing to the length of the expressions scaling with N , the sequence of operation to form the system of equations is reversed with orthogonality applied first followed by assembly. The system of equations is solved using the *LinearSolve* command in MAPLE[©]. In consonance with [41], the problem in Fig. 3d is solved for $\nu = 1/3, M = 3/8, \alpha = \pi/4, r_1 = 0.5, r_2 = 1, N = 250$ under plane stress conditions. Three values of inhomogeneity parameter $\beta = \{-2, 0, 2\}$ are considered with the result corresponding to the middle value compared with [41] while for $\beta \neq 0$, the results of the present work are compared with ABAQUS based FE results. The former will be referred to as Singh(2019) in the plots. The FE mesh for the MBV problem in Fig. 3d, constructed by employing the "Structured Mesh" feature in [47] comprises of 115378 CPS4 elements [47] such that the smallest element size is 0.005 along the radius $r = r_1$. Note that a combination of symmetric and antisymmetric terms in applied loading at the inner radius $r = r_1$ allows a thorough check of all the derived solutions and associated MAPLE[©] functions.

To start with, Fig. 8, 9 compares the in-plane stress and displacement components along the outer radius $r = r_2$ extracted from the present work with Abaqus based FE result. Owing to the excessively large value of stress components at the singular point ($r = r_2, \theta = \{\alpha, 2\pi - \alpha\}$), the difference in result with β value at other locations along $r = r_2$ got concealed, thereby hindering any meaningful conclusion. Hence for the sake of clarity, Fig. 8 shows results of in-plane stress-components for $\beta = 2$ case alone. As seen in Fig. 8a, 8c, 9a, 9b, the primary requirement of boundary conditions i.e. traction free condition in the part $\alpha < \theta < 2\pi - \alpha$ and zero displacement in the constrained portion $0 < \theta < \alpha$ and $2\pi - \alpha < \theta < 2\pi$ are correctly captured. Stress component σ_θ (Fig. 8b) and displacement components $\{u_r, u_\theta\}$ (Fig.

9) in the traction free portion $\alpha < \theta < 2\pi - \alpha$ as predicted by the present work matches very well with [41] for $\beta = 0$ and FE result for $\beta \neq 0$. Greater the value of the inhomogeneity exponent β , stiffer the FGM is and hence the displacement is understandably smaller with increasing β . In the neighbourhood of the singular point ($r = r_2, \theta \rightarrow \alpha$, and $\theta \rightarrow 2\pi - \alpha$), as expected, stress components (Fig. 8a-c) exhibits very high frequency oscillations owing to the square root singularity with oscillating multipliers [41, 51].

The present work being semi-analytical is not able to explicitly spell out the mathematical form of the singularity but the oscillations in the solution signifies a signature of the lurking singularity. A variety of filtering schemes are available to smoothen out the oscillations in the Fourier solution. Fig. 8d shows the outcome of the application of Lanczos filtering scheme [41] as applied to the stress component σ_θ plotted along the outer radius $r = r_2$. It can be contrasted with Fig. 8b to appreciate the effect of filtering especially in the vicinity of the singular points. Elsewhere the oscillations are small and results with and without filtering are almost indistinguishable. Nevertheless, the oscillatory solution generated in the present work can be always smoothened out by schemes like Lanczos filtering. **Note that the oscillations observed in Figs. 8a,8b, 8c are all variants of the Gibbs phenomenon, which occurs when quantities of interest i.e. stress and/or displacement exhibit sudden jump in their values [48].** The correctness of the present solution is further reinforced through comparison of the tangential stress σ_θ and displacement components $\{u_r, u_\theta\}$ at the inner radius $r = r_1$ through Fig. 10a and 10b-c respectively. Similar to Fig. 10a and 10b-c, maintaining the loading, boundary conditions and geometry equal, with increasing β , due to enhanced stiffness, displacement decreases while stress rises in the FG annulus. Comparison and validation along a number of additional paths is also carried out but not shown here for lack of novelty and space.

The results in Fig. 9-10 are calculated for a reasonably large $N = 250$ to ensure high level of accuracy. In order to check the dependence of present solution on N , strain energy $\int_V 0.5\sigma_{ij}\varepsilon_{ij}dV$ [42-44], a global quantity is computed for problem in Fig. 3d as a function of N for $\beta = \{-2, 0, 2\}$. Applying Clayperon's theorem, strain energy per unit out-of-plane length (U) in the annulus can be expressed as [42-44],

$$U = \frac{r_1}{2} \int_0^{2\pi} [-p_1(\theta)u_r(r_1, \theta) - q_1(\theta)u_\theta(r_1, \theta)]d\theta. \quad (39)$$

Calculation as described in sub-section 4.3 and the current section is carried out for different N and strain energy per unit out-of-plane length (U) via Eq. 39 is computed. The result of the exercise is plotted in Fig. 11 as a semi-log plot for $\{-2, 0, 2\}$ superimposed with the result from [41] for $\beta = 0$. It is evident from Fig. 11, that the present method with value of $N > 50$ will lend reasonably accurate solution for field quantities in annulus subjected to MBCs of the type shown in Fig. 3d except possibly in and around the singular points.

6. Conclusions

The present work proposes a novel semi-analytical technique to calculate stress and displacement field in a linear elastic, isotropic, functionally graded annulus while being subjected to mixed boundary conditions. Shear modulus is assumed to exhibit power-law variation with radius while the Poisson's ratio is assumed constant. Planar infinitesimal deformation is assumed under quasi-static conditions and in the absence of body force. The salient features of the current technique comprises of two major steps. In the first step, closed form expression for stress and displacement field in the annulus is derived for terms in the periodic Fourier series in angular variable (θ) as radial and tangential loading at inner and outer radius of annulus. The expressions are coded in the form of MAPLE[©] functions. In the second step, the small strain-displacement relationship in polar co-ordinates is exploited to rewrite the mixed boundary conditions in terms of displacement and its gradients. Having the boundary conditions expressed solely in terms of displacement all along the annulus boundary allows use of orthogonality principle leading to a system of linear equations. The length of expressions in the first step scales with the number of terms dealt in Fourier series and becomes unmanageable if handled all at once. Hence in practice, the process of assembling solution corresponding to all the Fourier terms followed by orthogonality is reversed. The versatility of the technique is thoroughly demonstrated through three examples of traction boundary value problems and one mixed boundary value problem. As compared to numerical methods like finite element method, boundary element method, which can handle complicated material response and any geometry, the current method deals with a specific geometry and material response but scores in terms of semi-analytical nature of solution and savings in computational space and time. In the analytical domain, technique like complex variable method offers an

extremely powerful means in Elasticity to handle boundary conditions of all kinds over a variety of planar geometries but not on annulus. In case of mixed boundary value problem, the semi-analytical nature of the current work prohibits the clear deduction of nature of singularity but its presence and location can be unambiguously deciphered through the high frequency and high amplitude oscillations in the obtained solution, which is nonetheless accurate elsewhere in the annulus. The present work thus serves as a feasible option to solve boundary value problems over power-law functionally graded linear elastic annulus. Efforts are ongoing to apply the present approach to crack problems in annulus made up of power-law functional grading. Lastly, the assumption of constant Poisson's ratio used in the present work can be relaxed without sacrificing the semi-analytical nature if the spatial variation is power-law with specific exponent as done in [18, 35, 52].

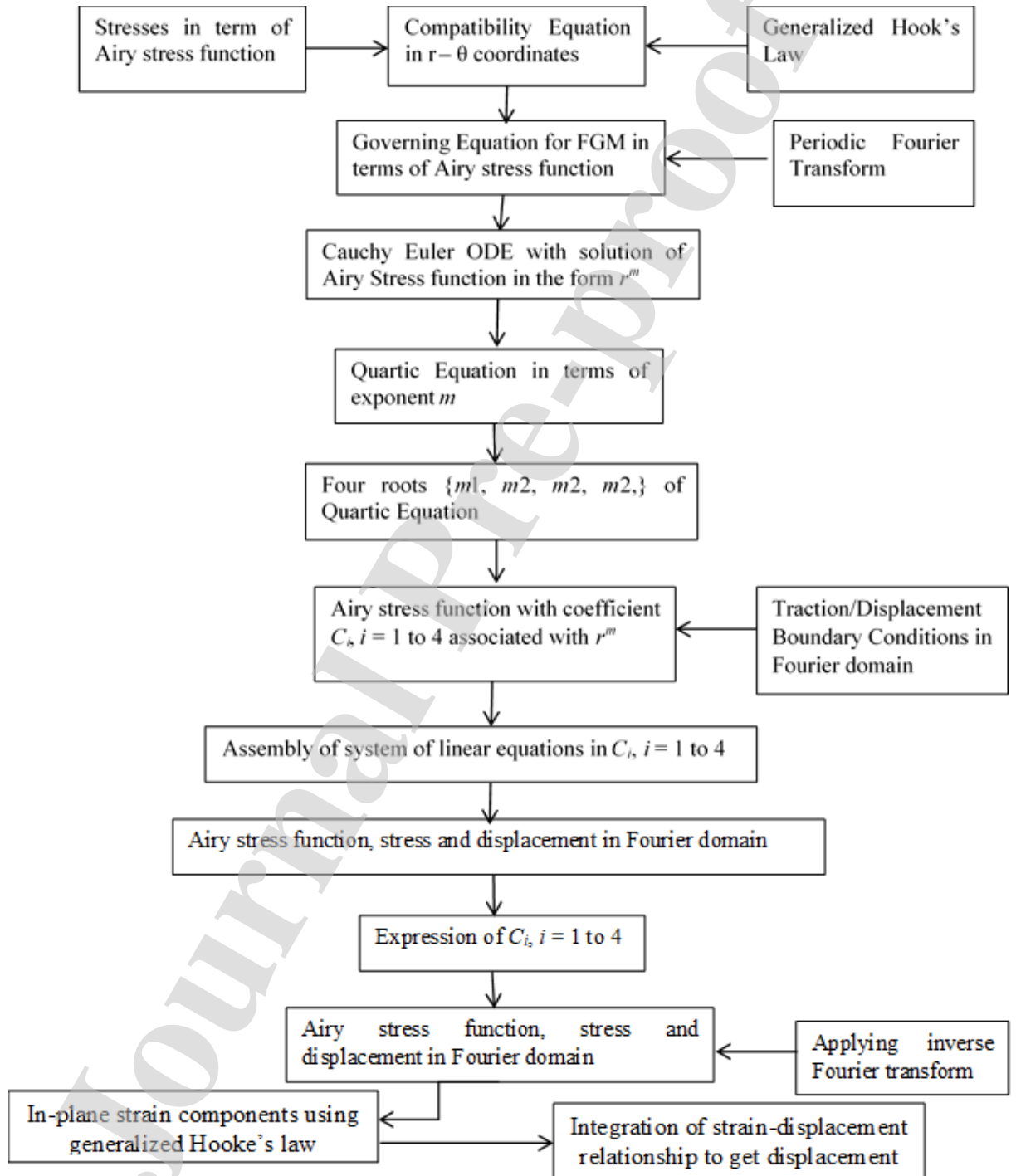


Figure 1: Flow chart for computing Airy stress function and planar stress and displacement components

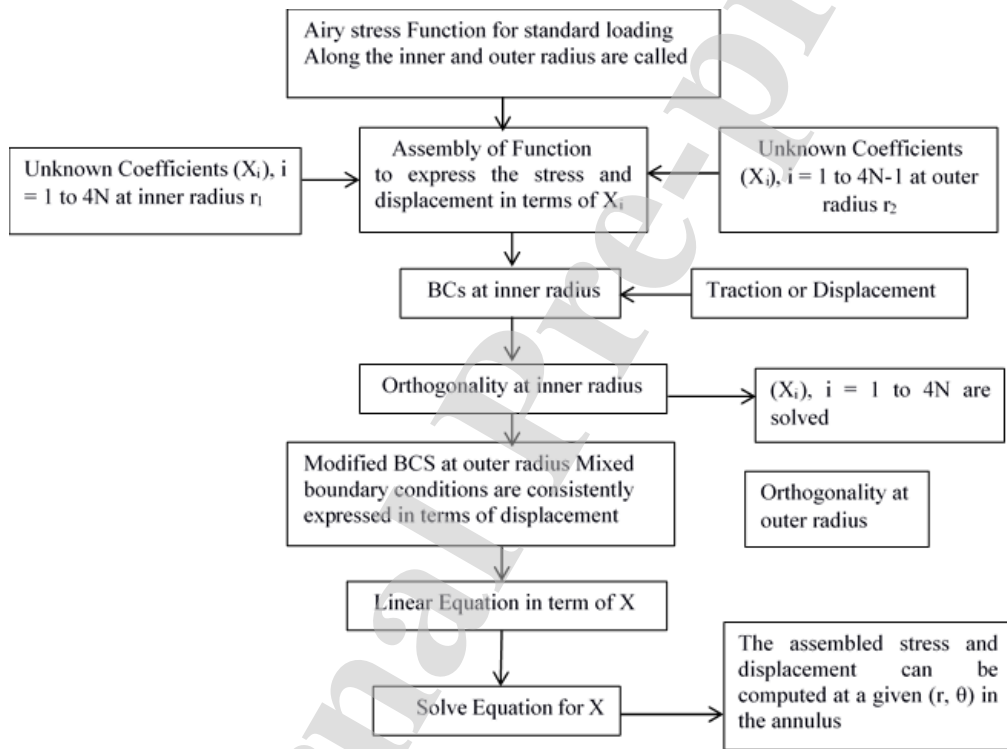


Figure 2: Flow chart of solution methodology for solving Mixed BVP in power-law graded linear elastic circular annulus (e.g. See Fig. 3d)

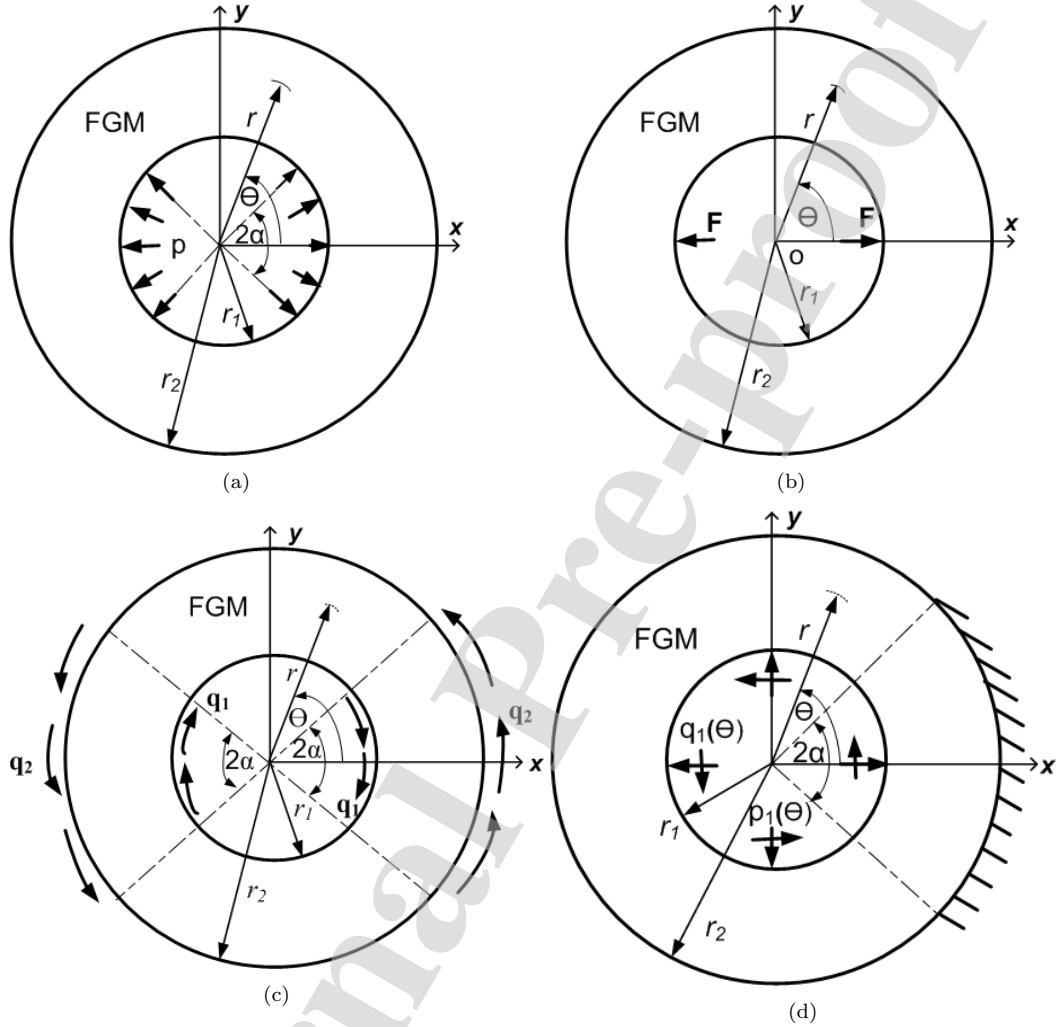


Figure 3: Functionally graded (FG) annulus of inner radius r_1 and outer radius r_2 made up of linear elastic isotropic material with constant Poisson's ratio ν and shear modulus $\mu(r)$ varying radially as $M(r/r_2)^\beta$, where β is the inhomogeneity parameter and M is the shear modulus at $r = r_2$. (a) Equal and opposite arcs along the inner surface $r = r_1$ symmetric about x -axis and subtending an angle 2α , subjected to uniform pressure p , (b) pair of equal and diametrically opposite horizontal point force per unit out-of-plane length F acting normal to the inner surface $r = r_1$, (c) equal and opposite arcs symmetric about x -axis and subtending an angle 2α being subjected to tangential traction q_1 along the inner surface $r = r_1$ and $q_2 = q_1(r_1/r_2)^2$ in the opposite sense along the outer surface $r = r_2$, (d) inner radius $r = r_1$ is subjected to radial traction $p_1(\theta)$ and tangential traction $q_1(\theta)$ while the outer radius $r = r_2$ is subjected to mixed boundary conditions i.e. displacement is constrained in the region $-\alpha < \theta < \alpha$ and the remaining portion $\alpha < \theta < 2\pi - \alpha$ is traction free.

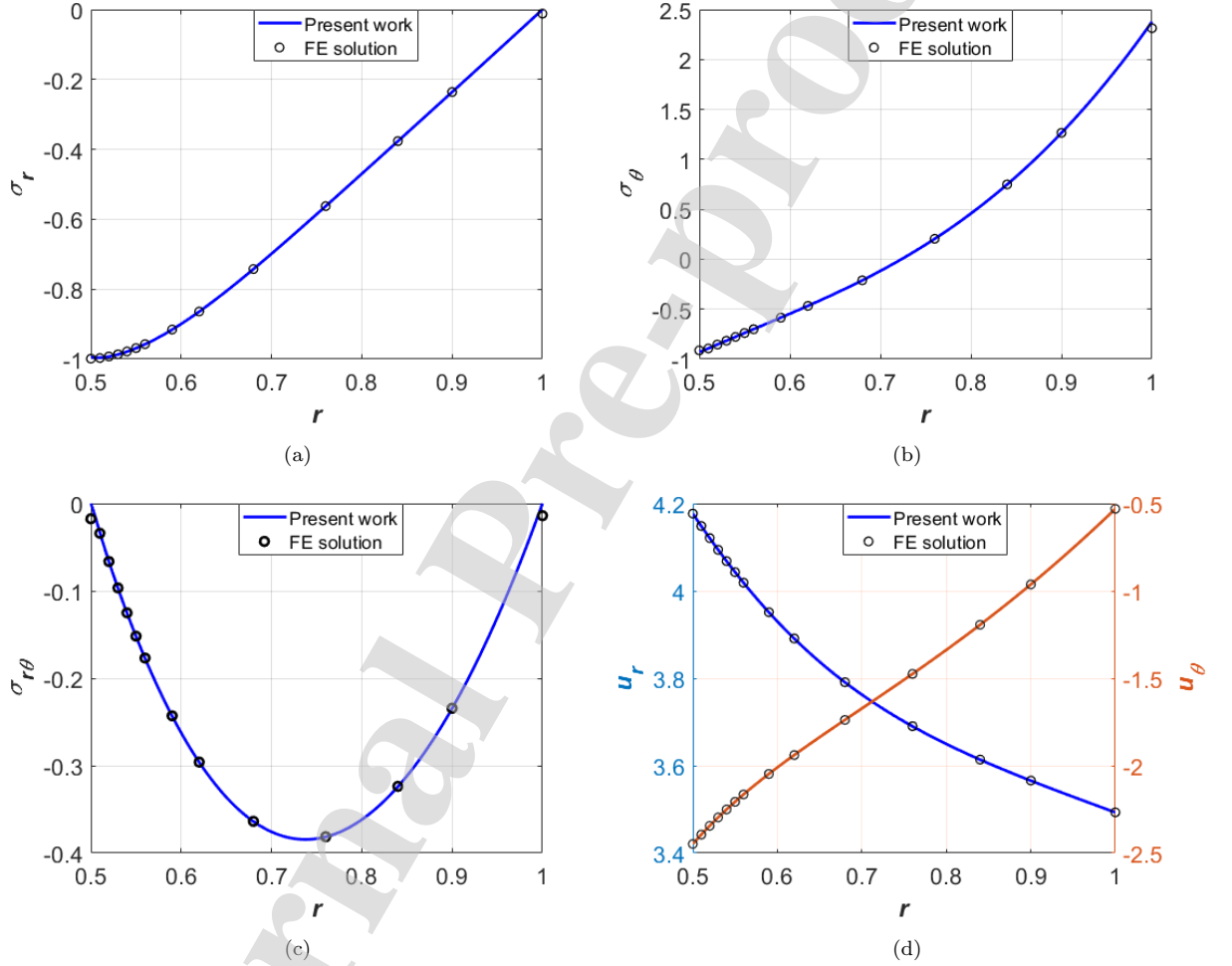


Figure 4: Comparison of in-plane component of (a) stress σ_r , (b) stress σ_θ , (c) stress $\sigma_{r\theta}$, (d) displacement $\{u_r, u_\theta\}$, along the radial path inclined at an angle of 21.36° with respect to the x -axis as obtained from the present work (continuous line) and Abaqus based FE solution (circular markers) for a power-law FG annulus (Eq. (1)) subjected to loading depicted in Fig. 3a under plane stress deformation. The pertinent numerical values are $p = 1, \alpha = \pi/4, M = 0.385, r_1 = 0.5, r_2 = 1, \nu = 0.3, \beta = 2, N = 100$.

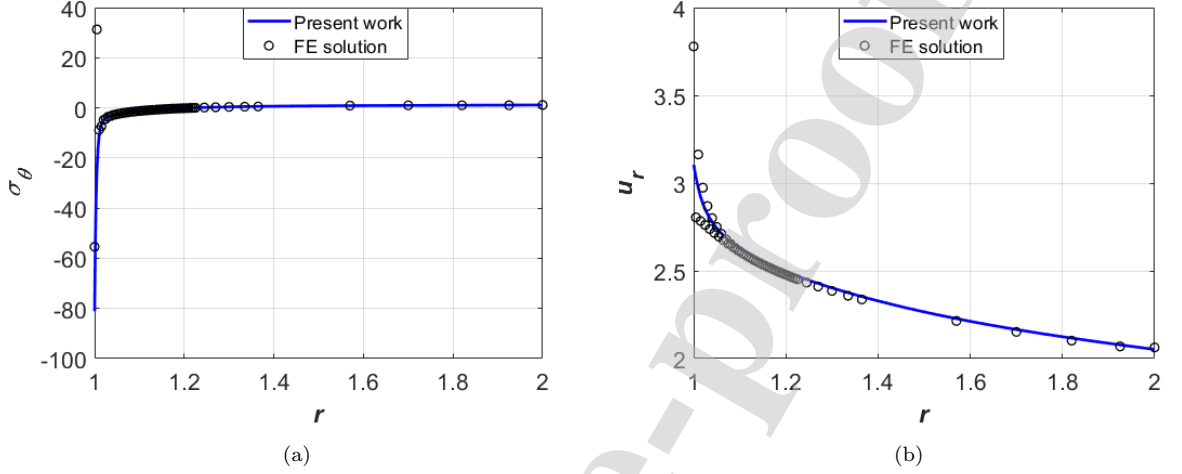


Figure 5: Comparison of tangential component of (a) stress σ_θ and (b) displacement u_θ , along the radial path coinciding with x -axis ($\theta = 0$) as obtained from the present work (continuous line) and Abaqus based FE solution (circular markers) for a power-law FG annulus (Eq. (1)) subjected to loading depicted in Fig. 3b under plane stress deformation. The pertinent numerical values are $F = 1$, $M = 0.385$, $r_1 = 1$, $r_2 = 2$, $\nu = 0.3$, $\beta = -2$, $N = 400$.

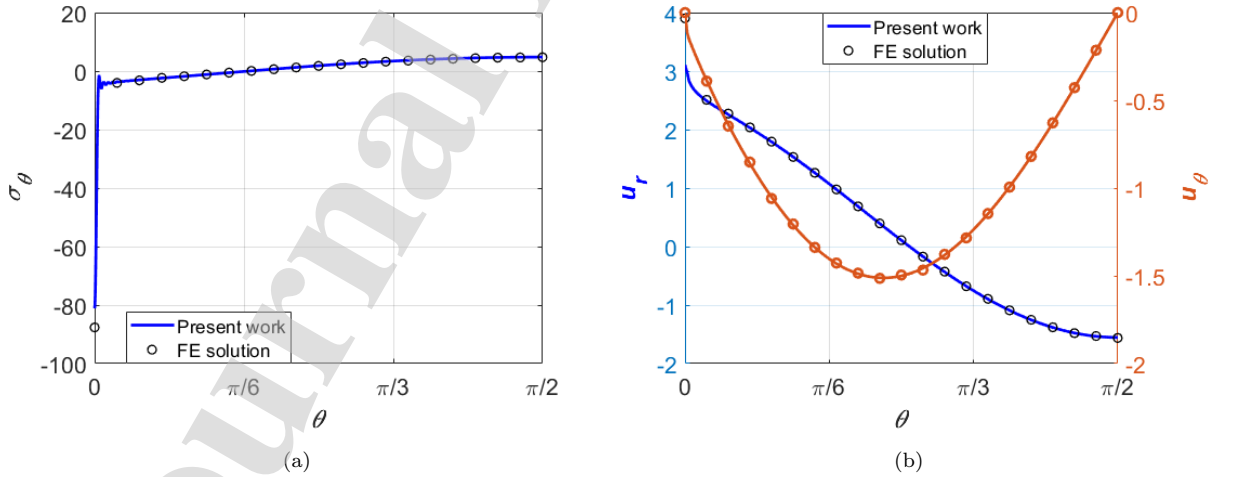


Figure 6: Comparison of (a) stress component σ_θ and (b) displacement components $\{u_r, u_\theta\}$, along the inner radius $r = r_1$ as obtained from the present work (continuous line) and Abaqus based FE solution (circular markers) for a power-law FG annulus (Eq. (1)) subjected to loading depicted in Fig. 3b under plane stress deformation. The pertinent numerical values are $F = 1$, $M = 0.385$, $r_1 = 1$, $r_2 = 2$, $\nu = 0.3$, $\beta = -2$, $N = 400$.

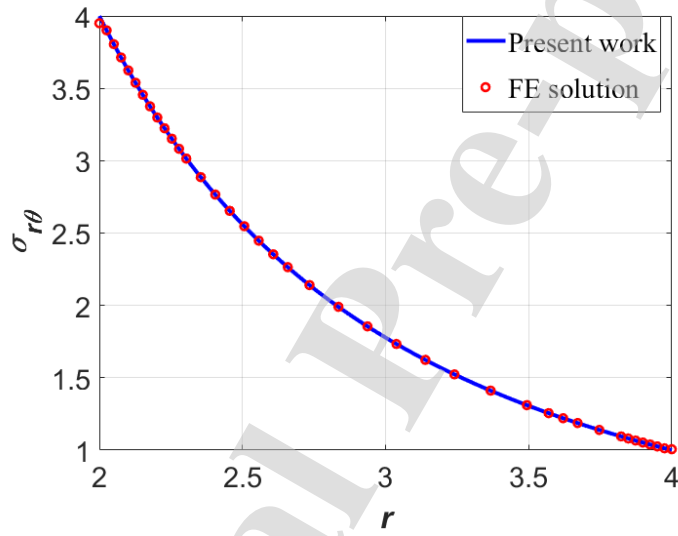


Figure 7: Comparison of stress component $\sigma_{r\theta}$ along the radial path coinciding with x -axis ($\theta = 0$) as obtained from the present work (continuous line) and Abaqus based FE solution (circular markers) for a power-law FG annulus (Eq. (1)) subjected to loading depicted in Fig. 3c under plane stress deformation. The pertinent numerical values are $\alpha = \pi/6$, $r_1 = 2$, $r_2 = 4$, $\beta = 1.5$, $M = 0.385$, $\nu = 0.3$, $N = 100$.

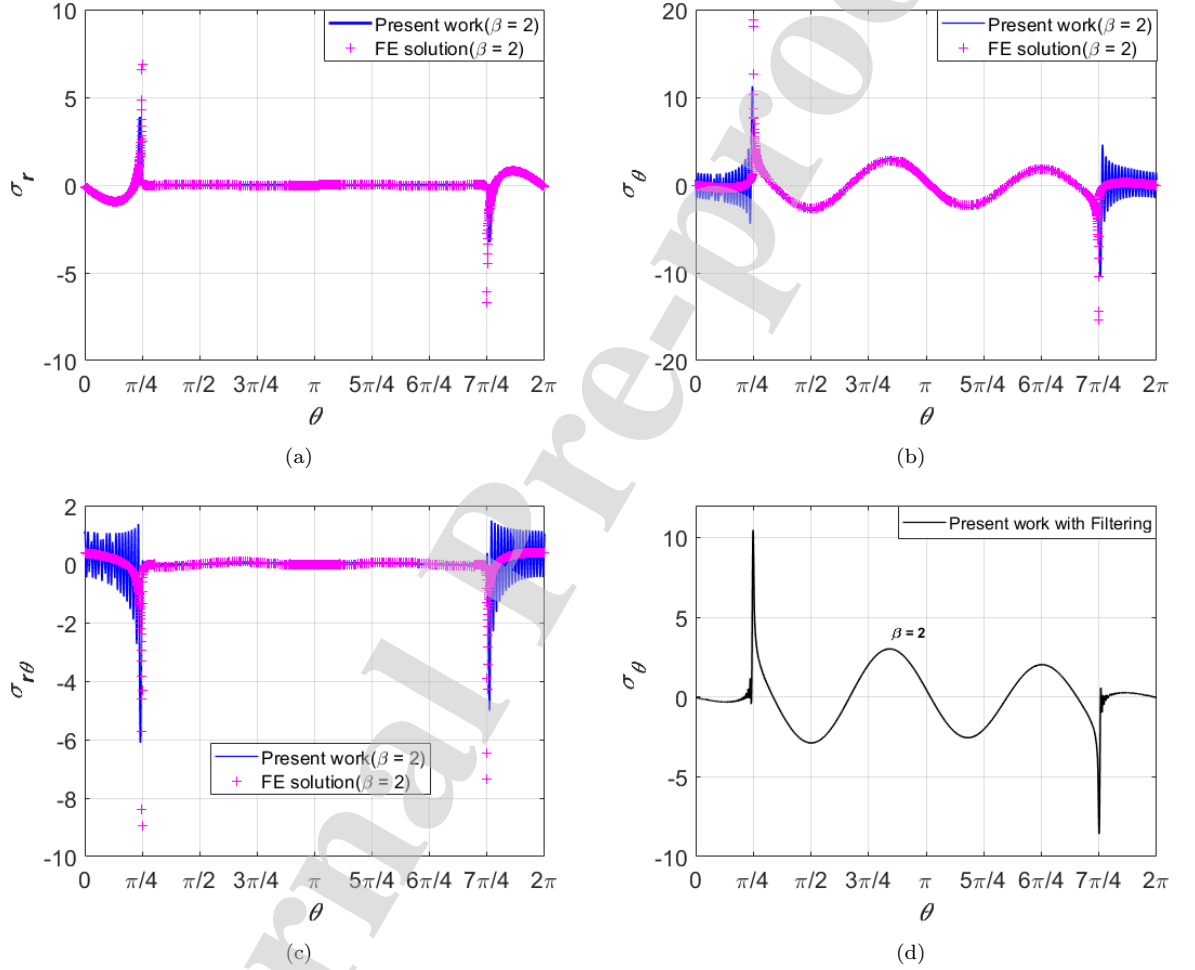


Figure 8: Effect of inhomogeneity parameter β on the variation of stress components (a) σ_r , (b) σ_θ , (c) $\sigma_{r\theta}$, (d) σ_θ after application of Lanczos filtering [41], along the outer radius $r = r_2$ for a power-law FG annulus subjected to loading depicted in Fig. 3d under plane stress conditions. The requisite details are $p_1(\theta) = \sin(3\theta) + \cos(2\theta)$, $q_1(\theta) = \cos(3\theta) + \sin(2\theta)$, $\nu = 1/3$, $M = 3/8$, $\alpha = \pi/4$, $r_1 = 0.5$, $r_2 = 1$, $N = 250$. FE result implies calculations carried out in commercial Finite element software ABAQUS.

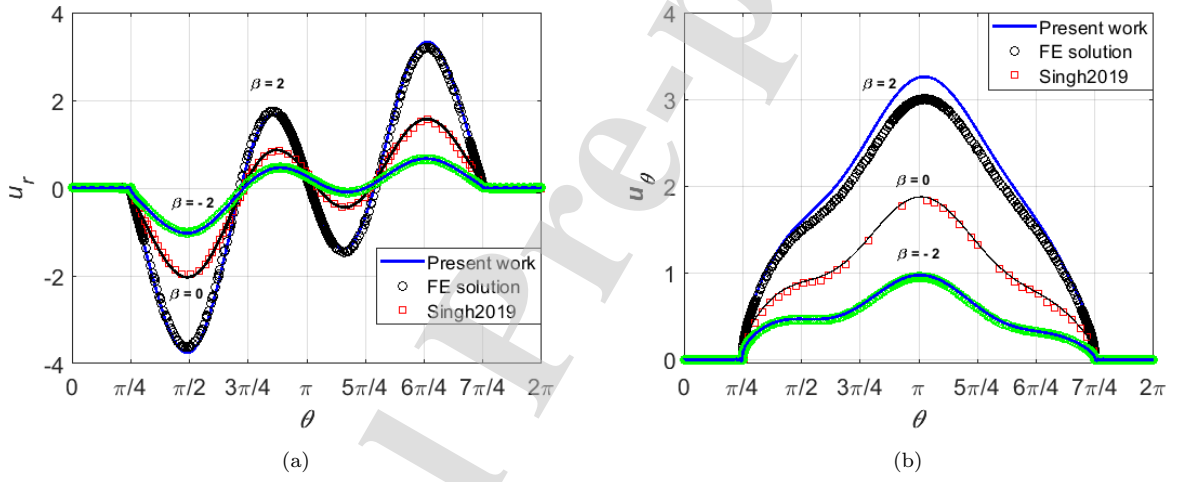


Figure 9: Effect of inhomogeneity parameter β on the variation of displacement components (a) u_r , (b) u_θ , along the outer radius $r = r_2$ for a power-law FG annulus subjected to loading depicted in Fig. 3d under plane stress conditions. The requisite details are $p_1(\theta) = \sin(3\theta) + \cos(2\theta)$, $q_1(\theta) = \cos(3\theta) + \sin(2\theta)$, $\nu = 1/3$, $M = 3/8$, $\alpha = \pi/4$, $r_1 = 0.5$, $r_2 = 1$, $N = 250$. Singh2019 denotes the result for homogeneous annulus ($\beta = 0$) from the work of Singh and Bhandakkar [41]. FE result implies calculations carried out in commercial Finite element software ABAQUS.

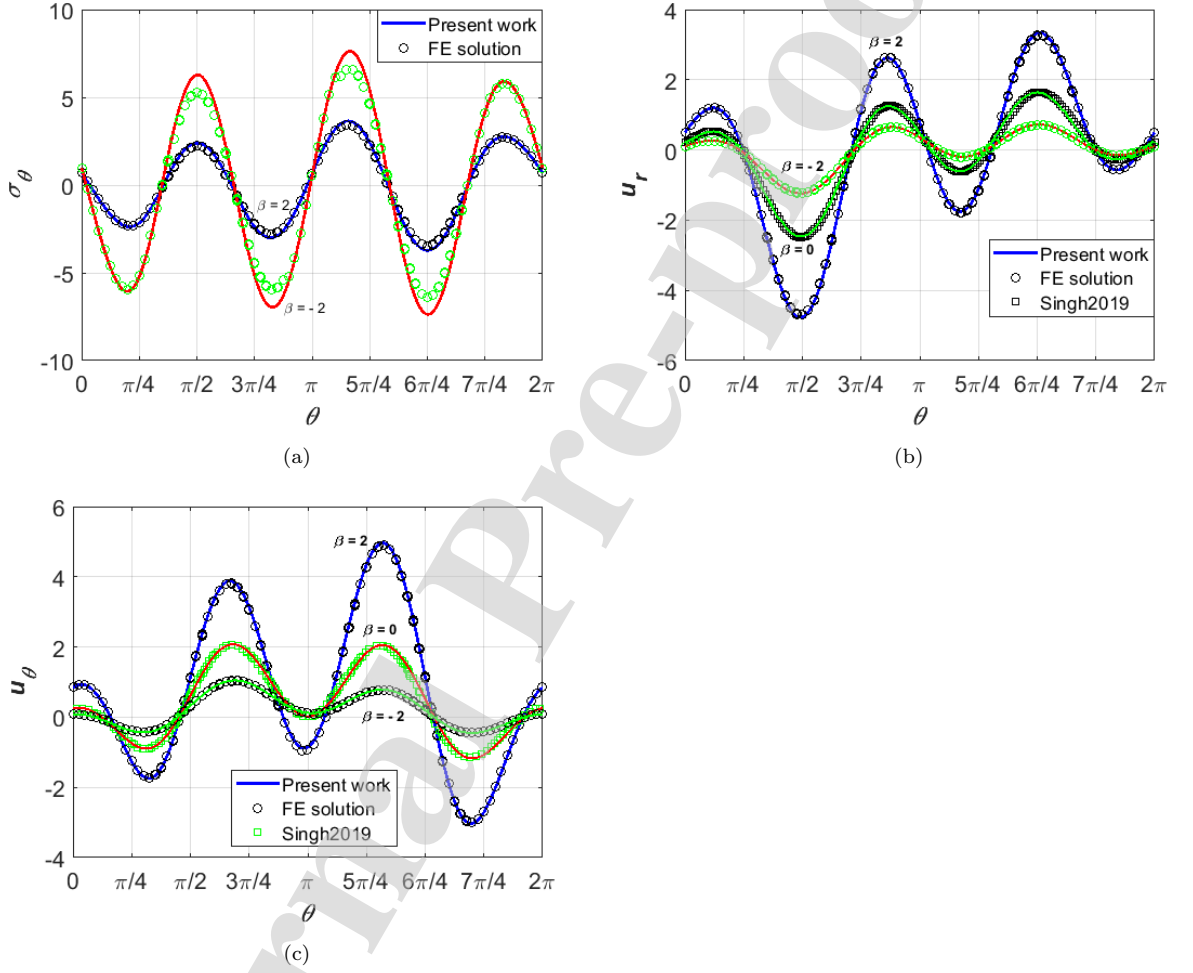


Figure 10: Effect of inhomogeneity parameter β on the variation of (a) tangential stress σ_θ , (b) radial displacement u_r , (c) tangential displacement u_θ , along the inner radius $r = r_1$ for a power-law FG annulus subjected to loading depicted in Fig. 3d under plane stress conditions. The requisite details are $p_1(\theta) = \sin(3\theta) + \cos(2\theta)$, $q_1(\theta) = \cos(3\theta) + \sin(2\theta)$, $\nu = 1/3$, $M = 3/8$, $\alpha = \pi/4$, $r_1 = 0.5$, $r_2 = 1$, $N = 250$. Singh2019 denotes the result for homogeneous annulus ($\beta = 0$) from the work of Singh and Bhandakkar [10]. FE result implies calculations carried out in commercial Finite element software ABAQUS.

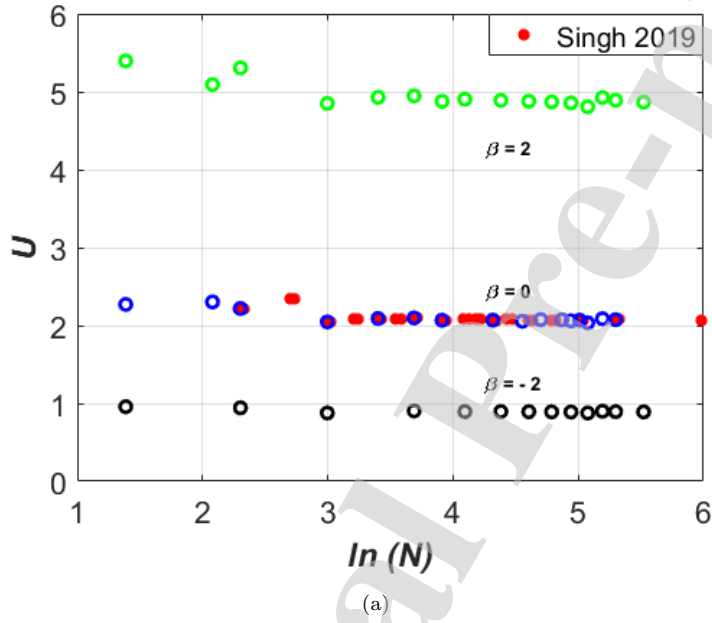


Figure 11: Variation of strain energy per unit out-of-plane length (U) with respect to the number of terms N in the periodic fourier series (Eq. 8) as a function of inhomogeneity parameter β for a power-law FG annulus subjected to loading depicted in Fig. 3d under plane stress conditions. The requisite details are $p_1(\theta) = \sin(3\theta) + \cos(2\theta)$, $q_1(\theta) = \cos(3\theta) + \sin(2\theta)$, $\nu = 1/3$, $M = 3/8$, $\alpha = \pi/4$, $r_1 = 0.5$, $r_2 = 1$, $N = 250$. Singh2019 denotes the result for homogeneous annulus ($\beta = 0$) from the work of Singh and Bhandakkar [41].

7. Appendix A: Modelling of FGM using ABAQUS

Usually the commercially available finite element programs doesnot offer in-built ready-made module to model FGMs. But the software programs can account for temperature dependent material properties. So the spatial variation intended for material properties is assigned to temperature and the material properties are made temperature dependent. Thus indirectly, the desired variation in material properties with spatial co-ordinates is acheived [50]. In this work, this technique is implemented in ABAQUS for shear modulus μ via assignment of temperature field in annulus which varies with radius as per Eq. 1. Note that the assigned temperature field is fictitious and hence the associated undesirable thermal deformation and stresses is prevented by enforcing the coefficient of thermal expansion to zero value.

References

- [1] A. E. T. Mahamood, Rasheedat Modupe, *Functionally graded materials*, Springer, (2017).
- [2] S. Suresh, Graded materials for resistance to contact deformation and damage, *Science* 292 (5526) (2001) 2447–2451.
- [3] M. R. Begley, N. R. Philips, B. G. Compton, D. V. Wilbrink, R. O. Ritchie, M. Utz, Micromechanical models to guide the development of synthetic brick and mortar composites, *Journal of the Mechanics and Physics of Solids* (60) (8) (2012) 1545–1560.
- [4] R. W. M. Niino, T. Hirai, The functionally gradient materials, *Journal of the Japan Society for Composite Materials* (13) (6) (1987) 257–264. .
- [5] E. Mueller, Č. Drašar, J. Schilz, W. Kaysser, Functionally graded materials for sensor and energy applications, *Materials Science and Engineering: A* (362) (1-2) (2003) 17–39.
- [6] Y. Zhang, Overview: damage resistance of graded ceramic restorative materials, *Journal of the European ceramic society* (32) (11) (2012) 2623–2632.
- [7] F. Watari, A. Yokoyama, M. Omori, T. Hirai, H. Kondo, M. Uo, T. Kawasaki, Biocompatibility of materials and development to functionally graded implant for bio-medical application, *Composites Science and Technology* (64) (6) (2004) 893–908.
- [8] W. Pompe, H. Worch, M. Epple, W. Friess, M. Gelinsky, P. Greil, U. Hempel, D. Scharnweber, K. Schulte, Functionally graded materials for biomedical applications, *Materials Science and Engineering: A* (362) (1-2) (2003) 40–60.
- [9] L. Lu, M. Chekroun, O. Abraham, V. Maupin, G. Villain, Mechanical properties estimation of functionally graded materials using surface waves recorded with a laser interferometer, *NDT & E International* (44) (2) (2011) 169–177.
- [10] L. B. Freund, S. Suresh, *Thin film materials: stress, defect formation and surface evolution*, Cambridge university press, (2004).

- [11] K. K. Chawla, Composite materials: science and engineering, Springer Science & Business Media, (2012).
- [12] Z. Shi, T. Zhang, H. Xiang, Exact solutions of heterogeneous elastic hollow cylinders, *Composite structures* (79) (1) (2007) 140–147.
- [13] X. Li, Y. Hua, C. Zheng, C. Mi, Tuning stress concentrations through embedded functionally graded shells, *Journal of Mechanics of Materials and Structures* (13) (3) (2018) 311–335.
- [14] H. Li, J. Lambros, B. Cheeseman, M. Santare, Experimental investigation of the quasi-static fracture of functionally graded materials, *International Journal of Solids and Structures* (37) (27) (2000) 3715–3732.
- [15] M. Hossain, C.-J. Hsueh, B. Bourdin, K. Bhattacharya, Effective toughness of heterogeneous media, *Journal of the Mechanics and Physics of Solids* (71) (2014) 15–32.
- [16] S. Brach, M. Hossain, B. Bourdin, K. Bhattacharya, Anisotropy of the effective toughness of layered media, *Journal of the Mechanics and Physics of Solids* (131) (2019) 96–111.
- [17] T. S. Vasu, T. K. Bhandakkar, Plane strain cylindrical indentation of functionally graded half-plane with exponentially varying shear modulus in the presence of residual surface tension, *International Journal of Mechanical Sciences* (135) (2018) 158–167.
- [18] G. Nie, R. Batra, Exact solutions and material tailoring for functionally graded hollow circular cylinders, *Journal of Elasticity* (99) (2) (2010) 179–201.
- [19] G. Nie, Z. Zhong, R. Batra, Material tailoring for functionally graded hollow cylinders and spheres, *Composites Science and Technology* (71) (5) (2011) 666–673.
- [20] J. Dryden, R. C. Batra, Optimum young's modulus of a homogeneous cylinder energetically equivalent to a functionally graded cylinder, *Journal of Elasticity* (110) (1) (2013) 95–110.
- [21] M. Kashtalyan, M. Menshykova, Three-dimensional elastic deformation of a functionally graded coating/substrate system, *International Journal of Solids and Structures* (44) (16) (2007) 5272–5288.

- [22] R. Sburlati, Analytical elastic solutions for pressurized hollow cylinders with internal functionally graded coatings, *Composite Structures* (94) (12) (2012) 3592–3600.
- [23] R. Sburlati, S. R. Atashipour, S. Hosseini-Hashemi, Study on the effect of functionally graded coating layers on elastic deformation of thick circular plates: a closed-form elasticity solution, *Composite Structures* (99) (2013) 131–140.
- [24] P. Chu, X.-F. Li, J.-X. Wu, K. Lee, Two-dimensional elasticity solution of elastic strips and beams made of functionally graded materials under tension and bending, *Acta Mechanica* (226) (7) (2015) 2235–2253.
- [25] R. Sburlati, S. R. Atashipour, S. A. Atashipour, Reduction of the stress concentration factor in a homogeneous panel with hole by using a functionally graded layer, *Composites Part B: Engineering* (61) (2014) 99–109.
- [26] Q. Yang, C.-F. Gao, Reduction of the stress concentration around an elliptic hole by using a functionally graded layer, *Acta Mechanica* (227) (9) (2016) 2427–2437.
- [27] H. Li, Y. Liu, Functionally graded hollow cylinders with arbitrary varying material properties under nonaxisymmetric loads, *Mechanics Research Communications* (55) (2014) 1–9.
- [28] X.-F. Li, X.-L. Peng, A pressurized functionally graded hollow cylinder with arbitrarily varying material properties, *Journal of Elasticity* (96) (1) (2009) 81–95.
- [29] M. Jabbari, A. Bahtui, M. Eslami, Axisymmetric mechanical and thermal stresses in thick long fgm cylinders, *Journal of Thermal Stresses* (29) (7) (2006) 643–663.
- [30] M. Jabbari, M. Meshkini, M. Eslami, Nonaxisymmetric mechanical and thermal stresses in fgppm hollow cylinder, *Journal of Pressure Vessel Technology* (134) (6) (2012) 061212.
- [31] C. Horgan, A. Chan, The pressurized hollow cylinder or disk problem for functionally graded isotropic linearly elastic materials, *Journal of Elasticity* (55) (1) (1999) 43–59.

- [32] E. Pan, A. Roy, A simple plane-strain solution for functionally graded multilayered isotropic cylinders, *Structural Engineering and Mechanics* (24) (6) (2006) 727–740.
- [33] A. S. Moghaddam, M. Alfano, R. Ghajar, Determining the mixed mode stress intensity factors of surface cracks in functionally graded hollow cylinders, *Materials & Design* (43) (2013) 475–484.
- [34] M. Jabbari, A. Bahtui, M. Eslami, Axisymmetric mechanical and thermal stresses in thick short length fgm cylinders, *International Journal of pressure vessels and piping* (86) (5) (2009) 296–306.
- [35] M. Mohammadi, G. Saha, A. Akbarzadeh, Elastic field in composite cylinders made of functionally graded coatings, *International Journal of Engineering Science* (101) (2016) 156–170.
- [36] O. C. Zienkiewicz, R. L. Taylor, P. Nithiarasu, J. Zhu, *The finite element method*, Vol. (3), McGraw-hill London, 1977.
- [37] P. K. Banerjee, R. Butterfield, *Boundary element methods in engineering science*, Vol. (17), McGraw-Hill London, 1981.
- [38] W. Xianfeng, N. Hasebe, Complex variable solution of plane problem for functionally graded materials, in: *IUTAM Symposium on Dynamics of Advanced Materials and Smart Structures*, (2003) 449–458.
- [39] A. H. England, *Complex variable methods in elasticity*, Courier Corporation, 2003.
- [40] V. Buchwald, A note on a method of milne-thomson, *Journal of the Australian Mathematical Society* (3) (1) (1963) 93–98.
- [41] G. Singh, T. K. Bhandakkar, Simplified approach to solution of mixed boundary value problems on homogeneous circular domain in elasticity, *Journal of Applied Mechanics* (86) (2) (2019) 021007.
- [42] R. W. Little, *Elasticity*, Prentice Hall, Englewood Cliffs, NJ.
- [43] J. Barber, *Elasticity* Springer (2004).

- [44] C. S. Jog, *Continuum Mechanics: Foundations and Applications of Mechanics*, 3rd ed., vol. 1, Cambridge University Press, New Delhi, India., (2015).
- [45] I. N. Sneddon, *Mixed boundary value problems in potential theory*.
- [46] D. Zill, W. S. Wright, M. R. Cullen, *Advanced engineering mathematics*, Jones & Bartlett Learning, 2011.
- [47] A. U. Manual, *Abaqus version 6.12-1 documentation*, Dassault Systemes SIMULIA Corporation, Providence, RI, USA.
- [48] C. Lanczos, *Applied analysis* prentice hall, New York.
- [49] S. Crouch, S. Mogilevskaya, Loosening of elastic inclusions, *International journal of solids and structures* (43) (6) (2006) 1638–1668.
- [50] T. Sadowski, M. Birsan, D. Pietras, Multilayered and fgm structural elements under mechanical and thermal loads. part i: Comparison of finite elements and analytical models, *Archives of civil and mechanical engineering* (15) (4) (2015) 1180–1192.
- [51] T. Ting, Asymptotic solution near the apex of an elastic wedge with curved boundaries, *Quarterly of Applied Mathematics* (42) (4) (1985) 467–476.
- [52] M. Mohammadi, J.R Dryden, Influence of the spatial variation of Poisson's ratio upon the elastic field in nonhomogeneous axisymmetric bodies, *International Journal of Solids and Structures*,(46) (3-4) (2009) 788-795.
- [53] M. Z. Nejad, M. Abedi, , M. H. Lotfian, M. Ghannad, Elastic analysis of exponential FGM disks subjected to internal and external pressure, *Central European Journal of Engineering*, (3)(2013) 459-465.
- [54] Y. Z. Chen, X. Y. Lin, Elastic analysis for thick cylinders and spherical pressure vessels made of functionally graded materials, *Computational Materials Science*, (44) (2) (2008) 581-587.
- [55] H. M, Wang, Elastic analysis of exponentially graded piezoelectric cylindrical structures as sensors and actuators, *Journal of Mechanical Science and Technology*, (26) (2012) 4047-4053.

- [56] A. Benslimane, S. Bouzidi, M. Methia, Displacements and stresses in pressurized thick-walled FGM cylinders: Exact and numerical solutions, *International Journal of Pressure Vessels and Piping*, 168, (2018) 219-224 .
- [57] H. Xiang, Z. Shi, T. Zhang, Elastic analyses of heterogeneous hollow cylinders, *Mechanics Research Communications*, 33(5) (2006), 681-691.
- [58] Y.Z. Chen, A novel numerical solution for a functionally graded hollow cylinder with arbitrary elastic property along the radial direction, *International Journal of Pressure Vessels and Piping*, Accepted, (2021).

Highlights:

- Closed form stress, displacement in power-law graded annulus for periodic loading
- Semi-analytical stress-displacement computation in annulus subjected to mixed BCs
- Potential to offer computationally efficient answer to fracture, material tailoring

Tanmay K. Bhandakkar: Conceptualization, Methodology, Supervision, Writing- Original draft preparation, Writing - Review & Editing.

Dinesh P. Chawde: Methodology, Software, Formal analysis, Data Curation, Investigation, Writing- Original draft preparation.

Journal Pre-proof

Declaration of interests

The authors declare that they have no known competing financial interests or personal relationships that could have appeared to influence the work reported in this paper.

The authors declare the following financial interests/personal relationships which may be considered as potential competing interests:

Journal Pre-proof